



**AN EXPERIMENTAL DESIGN FOR MEASURING IN SITU RADIATION
DAMAGE TO A PIEZOELECTRIC TRANSDUCER**

THESIS

Michael R. Severson, Major, USA

AFIT/GNE/ENP/04-06

**DEPARTMENT OF THE AIR FORCE
AIR UNIVERSITY**

AIR FORCE INSTITUTE OF TECHNOLOGY

Wright-Patterson Air Force Base, Ohio

APPROVED FOR PUBLIC RELEASE; DISTRIBUTION UNLIMITED

The views expressed in this thesis are those of the author and do not reflect the official policy or position of the United States Air Force, Department of Defense, or the United States Government.

AFIT/GNE/ENP/04-06

**AN EXPERIMENTAL DESIGN FOR MEASURING IN SITU RADIATION
DAMAGE TO A PIEZOELECTRIC TRANSDUCER**

THESIS

Presented to the Faculty

Department of Engineering Physics

Graduate School of Engineering and Management

Air Force Institute of Technology

Air University

Air Education and Training Command

In Partial Fulfillment of the Requirements for the

Degree of Master of Science (Nuclear Science)

Michael R. Severson, BS

Major, USA

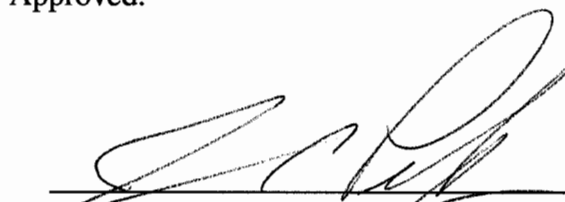
March 2004

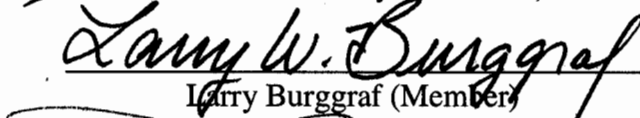
APPROVED FOR PUBLIC RELEASE; DISTRIBUTION UNLIMITED

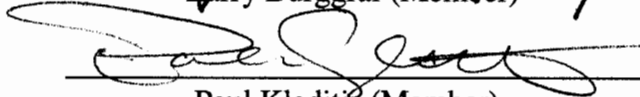
**AN EXPERIMENTAL DESIGN FOR MEASURING IN SITU RADIATION
DAMAGE TO A PIEZOELECTRIC TRANSDUCER**

Michael R. Severson, BS
Major, USA

Approved:


James C. Petrosky (Chairman)


Larry Burggraf (Member)


Paul Kladitis (Member)

12 MAR 04
Date

12 Mar 04
Date

12 MAR 04
Date

Abstract

An experiment was conducted investigating the use of an acoustic pulse waveguide to collect response measurements from three piezoelectric acoustic emission (AE) transducers while the transducers were exposed to an active nuclear reactor neutron flux ranging from 1×10^{11} to 2.4×10^{12} neutrons per $\text{cm}^2 \text{ s}$. Material, mechanical, and radiation studies were performed to determine a practical design for the construction of the experiment. Discrete frequency pulses generated by an Arbitrary Waveform Generator were transmitted by an aluminum waveguide to the core of the Ohio State University Research Reactor (OSURR). Three AE transducers coupled to the waveguide were exposed to the reactor neutron fluence and their response to each frequency pulse was measured over time. The recorded data was used to study the correlation between the neutron dose and resulting device damage. Response measurements were also taken in situ during post-irradiation periods to determine if response changes due to radiation damage would recover with time.

Data sampling of transducer response was reproducible with a standard deviation that ranged between 3% and 8% of the mean value for all frequencies. Final transducer response levels varied between devices and frequencies, but were consistently degraded. Decreases in response between transducers ranged from 36% to 78% using the average percent decrease over ten test frequencies. Individual frequency response degradation ranged from 16% to 92%.

Acknowledgments

I want to thank my advisor, LTC James Petrosky, for his support and guidance during this project. His enthusiasm and genuine interest in my progress helped keep me focused during the many distractions and discouragements that occurred in my laboratory research.

I could not have conducted this research without the generosity of Dr. Andrew Rosenberger, from the Air Force Research Laboratories. He provided the acoustic emission equipment that was used for data collection and without which there would have been no experiment. Thank you Andy.

Dr. Steve McCready of Los Alamos National Laboratories was very helpful in providing equipment for my work and insights regarding the motivation for using the devices that were the subject of the research. I thank him for taking time from a very busy schedule to spend with me.

I thank my father for his earnest support and words of encouragement. I am sure if I had asked, he would have flown down from Alaska to personally help me complete this project.

Most importantly, I thank my wife for accepting the extra burdens that are attached to attending AFIT. Her support and devotion over the last two years has helped me immeasurably in completing my studies and I am truly blessed to have her by my side.

Michael R. Severson

Table of Contents

	Page
Abstract.....	iv
Acknowledgments.....	v
List of Figures	viii
List of Tables	xii
I. Introduction	1
Background.....	1
Problem Statement.....	5
Research Scope.....	6
Methodology.....	7
Assumptions/Limitations.....	7
II. Theory	9
Chapter Overview.....	9
Material Study	9
Mechanics Study	15
Transducers.....	15
Acoustics.	19
Thermal Effects.	22
Coupling.	23
Radiation Study	24
Dose Determination.....	24
Damage Mechanisms.....	26
Activation.	29
Noise Generation.....	30
III. Experimental Design.....	32
Equipment and Test Station Configuration	32
Waveguide Construction	35
Data Sampling Method.....	38
Measurement System Characterization	42
Experimental Procedure	52

IV. Results and Analysis	54
Thermal Effects	54
Irradiation Results	56
Initial Phase Radiation Response.	59
Intermediate Phase Radiation Response.....	60
Final Phase Radiation Response.....	60
V. Conclusions and Recommendations	63
Conclusions	63
Recommendations	65
Appendix A: Irradiation Data	68
Appendix B: Relative Response Change by Frequency	73
Appendix C: Macroscopic Cross Section for Lead Metaniobate	89
Appendix D: Total Dose Calculation.....	90
Appendix E: Rate of Heating for Lead Metaniobate	93
Appendix F: Heat Transfer Calculations.....	94
Bibliography	97
Vita	100

List of Figures

Figure	Page
1. ACRR core control diagram	2
2. Induced dipole in piezoelectric material	10
3. Polarizing (poling) a piezoelectric ceramic (Piezoelectricity, 2004).....	12
4. Direction of forces affecting a piezoelectric element (Piezoelectricity, 2004).....	13
5. Piezoelectric transducer (Piezoelectric Transducers, 2003)	17
6. Acoustic source signal (bottom) and transducer response (top)	22
7. Thermal effect on transducer response	22
8. Displacement damage in crystal lattice.....	28
9. Experiment test station configuration	32
10. Relative size of pulser (left) and transducer (right)	33
11. Cross section of B1025 AE transducer	34
12. Wave guide apparatus	37
13. Frequency sweep from 1 kHz to 500 kHz with source signal (bottom) compared to response signal (top)	39
14. Transducer response to 600 kHz acoustic pulse	40
15. 100 kHz response data file.....	41
16. B1025 transducer response precision with 1 standard deviation error bars.....	42
17. Waveguide and transducers	43
18. Waveguide and transducers	43
19. Pulser connection to waveguide.....	44

20. Bench characterization of transducers at 24°C	44
21. Thermal characterization	47
22. Transducer response change at 100°C	48
23. Thermal heating of transducer sn9 with couplant.....	51
24. Thermal heating of transducer sn9 without couplant.....	51
25. In situ characterization	52
26. Thermal heating of transducer sn9 with couplant.....	55
27. Thermal heating of transducer sn9 without couplant.....	55
28. Irradiation response at 400 kHz	57
29. Irradiation response at 900 kHz	57
30. In situ characterization	58
31. Neutron damage mechanism.....	59
32. Transient effect caused by ionizing radiation	61
33. Irradiation response at 100 kHz	69
34. Irradiation response at 200 kHz	69
35. Irradiation response at 300 kHz	70
36. Irradiation response at 500 kHz	70
37. Irradiation response at 600 kHz	71
38. Irradiation response at 700 kHz	71
39. Irradiation response at 800 kHz	72
40. Irradiation response at 1 MHz.....	72
41. C1 lower frequency response change at 50 kW.....	74

42. C2 lower frequency response change at 50 kW	74
43. C3 lower frequency response change at 50 kW	75
44. C1 higher frequency response change at 50 kW	75
45. C2 higher frequency response change at 50 kW	76
46. C3 higher frequency response change at 50 kW	76
47. C1 lower frequency response change at 100 kW	77
48. C2 lower frequency response change at 100 kW	77
49. C3 lower frequency response change at 100 kW	78
50. C1 higher frequency response change at 100 kW	78
51. C2 higher frequency response change at 100 kW	79
52. C3 higher frequency response change at 100 kW	79
53. C1 lower frequency response change at 450 kW on day 2	80
54. C2 lower frequency response change at 450 kW on day 2	80
55. C3 lower frequency response change at 450 kW on day 2	81
56. C1 higher frequency response change at 450 kW on day 2	81
57. C2 higher frequency response change at 450 kW on day 2	82
58. C3 higher frequency response change at 450 kW on day 2	82
59. C1 lower frequency response change at 450 kW on day 3	83
60. C2 lower frequency response change at 450 kW on day 3	83
61. C3 lower frequency response change at 450 kW on day 3	84
62. C1 higher frequency response change at 450 kW on day 3	84
63. C2 higher frequency response change at 450 kW on day 3	85

64. C3 higher frequency response change at 450 kW on day 3	85
65. C1 lower frequency response change at 450 kW on day 4	86
66. C2 lower frequency response change at 450 kW on day 4	86
67. C3 lower frequency response change at 450 kW on day 4	87
68. C1 higher frequency response change at 450 kW on day 4	87
69. C2 higher frequency response change at 450 kW on day 4	88
70. C3 higher frequency response change at 450 kW on day 4	88
71. Pb206 dose rate calculation at 300 kW	90
72. Pb206 dose calculation at all powers used in reactor.	91
73. Total dose to lead metaniobate.	92

List of Tables

Table	Page
1. Lead Metaniobate Physical/Electrical Properties	14
2. Typical Sensor Specifications (Holbert, short course, 2004)	16
3. B1025 Transducer Specifications	18
4. Fundamental frequency for various metals.....	20
5. Average transducer response decrease.....	49
6. Transducer tracking sheet	49
7. Neutron fluence as a function of time.....	58
8. Irradiation schedule.....	68

AN EXPERIMENTAL DESIGN FOR MEASURING IN SITU RADIATION DAMAGE TO A PIEZOELECTRIC TRANSDUCER

I. Introduction

Los Alamos National Laboratory (LANL) has been performing experiments related to the nuclear stockpile stewardship program using the Annular Core Research Reactor (ACRR) located at Sandia National Laboratory (SNL) in New Mexico. The experiment involves exposing the contents of a sealed metal containment vessel to a radiation pulse being generated by the ACRR. The radiation pulse produces a pressure induced shockwave that propagates through the metal containment vessel. Researchers at LANL, in conjunction with Arizona State University (ASU), are interested in measuring the propagation of the shockwave and are currently investigating the use of piezoelectric acoustic emission transducers to collect data (Holbert et. al., 2003, 2-5).

Background

The ACRR is a water moderated, convective cooling pool-type reactor. The core consists of uranium oxide (UO_2) in combination with beryllium dioxide (BeO_2) and is enriched to 35 wt% ^{235}U . It has a steady-state power capability of 2-4 $\text{MW}_{(\text{th})}$ and a maximum pulse capability of 35,000 $\text{MW}_{(\text{th})}$ peak power in a 7 ms time interval.

The ACRR pulse mode is initiated by nitrogen pressure ejection of the transient rods resulting in an immediate power surge. The power surge causes the core (figure 1)

temperature to increase resulting in fuel expansion, also known as negative temperature feedback. Decreased fuel density diminishes the neutron chain reaction rate in the core resulting in a sharp decrease in power. A rapid safety shutdown, also called “scram”, is executed immediately following the energy pulse by inserting safety rods into the core. Insertion of the safety rods increases non-fission neutron absorption reactions and, in combination with the negative temperature feedback, results in the core becoming sub-critical.

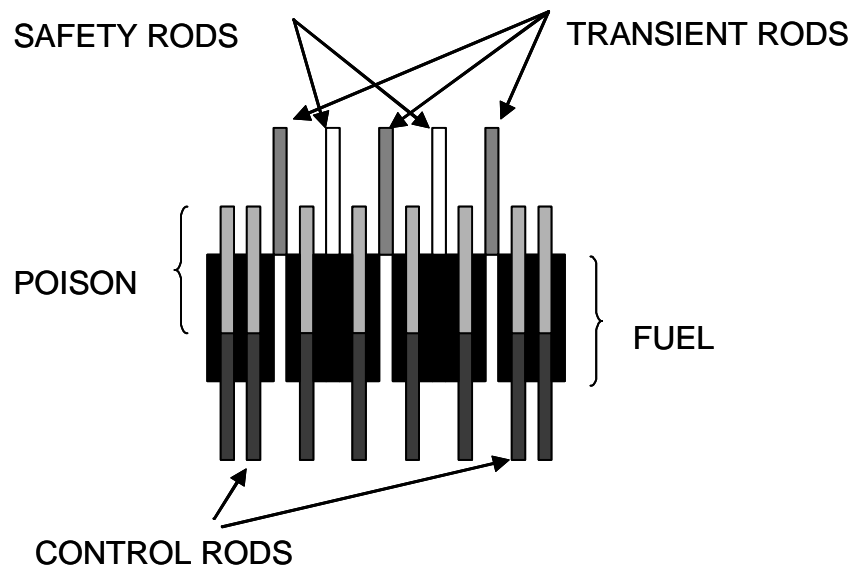


Figure 1. ACRR core control diagram

Conducting experiments in a high-energy pulsed reactor environment creates additional challenges to data collection when using sensors constructed from semiconductor materials. Semiconductors are susceptible to damage from exposure to

high levels of both ionizing and non-ionizing radiation. The research being conducted at LANL and ASU has encountered considerable difficulty in acquiring a piezoelectric or piezoresistive transducer that is not damaged by the pulsed radiation environment in the ACRR. They have observed that some transducers fail initialization tests after being in a storage vault for several months and exposed to a gamma flux of $10^5 \text{ cm}^{-2} \text{ s}^{-1}$. Some transducer models fail after being exposed to a single reactor pulse while others survive multiple reactor pulses (McCready et. al., 2003, 1-5).

Piezoresistive transducers rely on conductivity changes in a reference material that is subjected to stress. If an electric potential is applied across a piezoresistive material in an electrical circuit and a pressure differential is applied, the measured current will vary with the applied pressure. This type of transducer requires an applied potential and electrical current to be useful for pressure measurement. In an ionizing radiation environment, its performance will be degraded by induced currents and conductivity changes in insulating materials.

Piezoelectric transducers are small, lightweight, simply constructed, and do not require an applied potential or electrical current to perform measurements. Piezoelectric materials generate an electric potential in response to an applied force and the potential generated is proportional to the force. Transducers constructed from piezoelectric ceramic materials may offer an ionizing-radiation hardened alternative to silicon-based transducers because they do not rely on electrical current to measure applied force. Research conducted on lithium niobate exposure to gamma irradiation indicated no

significant change in piezoelectric properties up to a total dose of 10^{10} Roentgen, or approximately 10^4 Mrad (Halverson et. al., 1970, 335; Smith, 1971, 713).

Lead metaniobate (PbNb_2O_6) is a ceramic material that has some particularly attractive properties for use in a piezoelectric transducer. It has a high melting point suggesting a potential for high temperature operation and a broad range of frequency response. It also has a very high electromechanical coupling (0.6), which is the ratio of energy absorbed to that converted to a piezoelectrical response (Broomfield, 1985, 8).

Recently, ASU tested certain ceramic acoustic emission (AE) transducers composed of lead metaniobate. Acoustic emission occurs when a material subjected to stress releases energy in the form of an acoustic wave. Different materials have characteristic acoustic emission frequencies. Acoustic emission sensors are piezoelectric transducers which are capable of detecting a very broad band of frequencies. Frequency information measured by the transducer can then be used to determine the material composition of the source. It is also possible to identify the location of a frequency source by using multiple AE transducers at various locations on an object. By capturing time of frequency arrival, triangulation techniques can be used to determine location.

The sensors were exposed to 4.5 Mrad of ionizing radiation in a ^{60}Co gamma cell and continued to measure acoustic signals without experiencing degraded performance (Holbert et. al., 2003, 2-5). However, performance was not measured in situ and the ACRR generates both gamma and neutron radiation. In order to substantiate the radiation tolerance of lead metaniobate AE transducers, it is essential to subject the sensors to neutron irradiation and determine if there is any performance degradation in situ.

Following an extensive literature search, it became apparent that very little work exists dedicated to examining the effects of non-ionizing radiation on piezoelectric materials. There is even less available information concerning neutron irradiation of lead metaniobate and resultant displacement damage.

This research is an initial investigation into the behavior and performance of lead metaniobate as an acoustic emission sensor material in a non-ionizing radiation environment. It will examine the relationship between neutron radiation dose and its impact on the performance of lead metaniobate piezoelectric acoustic emission transducers.

Problem Statement

Previous research of radiation effects on AE transducers at LANL and ASU has been isolated to gamma radiation environments and has not included neutrons. The transducers will be used in the ACRR to take AE measurements during a radiation pulse, which will result in their exposure to a neutron fluence of 10^{15} cm^{-2} . An understanding of the effects of neutron damage on the operation of these transducers is essential to the success of the LANL research.

The goals of this research are: (1) to construct an experimental apparatus that will generate reproducible in situ response measurements for a range of acoustic pulse transmissions using lead metaniobate AE transducers in close proximity to the core of a nuclear reactor, (2) characterize the relationship between neutron radiation exposure and frequency sensitivity of the transducers, (3) determine if there is a radiation dose limit where the transducers fail to give a reproducible response with a standard deviation that

is less than 10% of the mean value measured, and (4) investigate response recovery of the transducers to neutron radiation damage at ambient room temperature.

Research Scope

This research will investigate an experimental design for in situ measurements of the effects of neutron radiation on piezoelectric devices. The emphasis of the research is to gather accurate and consistently reproducible data on the response of a lead metaniobate transducer as a function of long term exposure to neutron radiation. Piezoelectric AE transducers are to be used by Los Alamos National Laboratory (LANL) to measure pressure changes in a high flux neutron environment, so it is necessary to understand the effects that neutron radiation will have on the operation of the transducers.

Prior research shows that using piezoresistive silicon transducers to measure a pressure induced shockwave traveling through the walls of a metal container inside the ACRR during a radiation pulse would have a high probability of failure. Displacement damage has been shown to cause resistivity changes in silicon based sensors of 3.7% during exposure to a neutron fluence one order of magnitude less than a pulse in the ACRR (Willmon, 2003, 52). Multiple piezoresistive transducers used in the ACRR facility have failed from low dose exposure to ionizing radiation (McCready, 2002, 5).

Alternatively, piezoelectric transducers are inherently more resistant to ionizing radiation. If it can be shown that neutron radiation does not cause transducer failure, AE transducers could be used in the ACRR during pulse experiments for shockwave measurement and for identifying the composition and location of the source of a measured frequency.

Methodology

The theory of this research focuses on three fields of physics which will influence the experimental design: A material study, a mechanics study and a radiation study. The conclusions from the studies combined with a thorough literature review will aid in selection of materials, construction of the experiment, and development of the procedures that will be used to ensure the research goals are successful.

The material study will focus on understanding the material used to construct the transducers. More specifically, the physical characteristics of lead metaniobate (PbNb_2O_6) will be emphasized because it is the piezoelectric material used in the acoustic emission transducers to be tested.

The mechanical study will investigate how transducers operate, the propagation of sound in solid media, how coupling affects transducer performance, and the effects of thermal heating on the transducers and materials used in this experiment.

Finally, the radiation study will focus on neutron radiation dose calculations, activation of materials used in constructing the experiment, noise generation, and radiation damage mechanisms.

Assumptions/Limitations

Permanent damage due to ionizing radiation will be considered negligible based on previous experimental work conducted by ASU and LANL. Data gathered by Holbert et. al. indicates that this assumption is legitimate for gamma doses up to 4.5 Mrad using a ^{60}Co gamma source at a dose rate of 2.5 krad per minute (Holbert, 2003, 3). Although this may not be a correct assumption, limited resources and time preclude an

investigation into the contribution of gamma radiation to the overall effect on the experiment.

II. Theory

Chapter Overview

This chapter investigates the influence that materials, mechanics, and radiation will have on the experiment. The information will be used as a guide in the selection of materials to construct the experiment and in the design of the experiment. The material study is concerned primarily with the theory of piezoelectric materials. The mechanical study will focus on the operating mechanics of transducers, thermal effects, coupling issues, and the concept of using a waveguide as a means of getting in situ response data from the transducers as they are being irradiated inside a nuclear reactor. The radiation study will review transducer radiation dose calculations, activation of materials, signal/noise considerations, and radiation damage mechanisms.

Material Study

Piezo is derived from a Greek word meaning “to press”, so piezoelectricity is electricity originating from pressure. Piezoelectricity appears only in insulating solids. There are several materials able to produce the effect but crystalline materials are the most common (Mason, 1950, 1). There are a number of piezoelectric materials which occur naturally. Some of the more common types include: quartz (SiO_2), tourmaline, and Rochelle salt. Although natural piezoelectric materials are still occasionally used, their performance is generally not as good as man-made ceramic piezoelectrics. These materials can be made with a very high degree of purity and can be tailored to meet the needs of a specific application.

The piezoelectric effect is caused by the application of stress on a crystal with no center of symmetry. The stress will induce an unsymmetrical separation of charges along the crystal lattice which causes the formation of a dipole moment (figure 2). When a periodic force is applied to a piezoelectric material, it will produce a voltage that is proportional to the force applied with the same frequency.

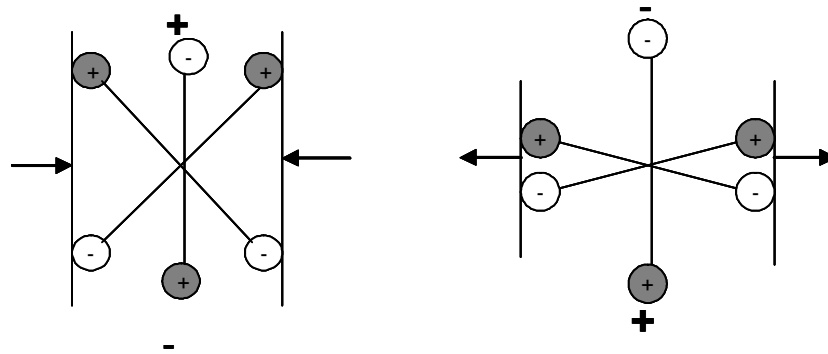


Figure 2. Induced dipole in piezoelectric material

Piezoelectric materials are often almost as rigid as a proportional piece of steel. Their inherent rigidity gives them a high natural frequency and a rapid rise time making them suitable for measuring quick or sharp forces such as high velocity impacts or high frequency vibrations. They are often used to measure rapidly changing pressures such as those resulting from blasts, explosions, and pulsations. To ensure measurement accuracy, the natural frequency of the sensor material must be considerably higher than the frequency to be measured or else measurement errors will result (Force Sensors, 2003).

Piezoelectric materials are considered to be ferroelectric in nature and also have the property of being pyroelectric. Ferroelectric materials have a permanent spontaneous electric polarization that can be reversed in an electric field. Although all piezoelectric materials are also ferroelectrics, the opposite does not apply. A ferroelectric substance may also have a center of symmetry which will result in no net dipole being formed in the crystal lattice.

A pyroelectric material is able to produce a state of electric polarity by a change of temperature. Pyroelectric crystals have a built-in permanent electric polarization which is compensated for by free charge carriers which have migrated to the crystal surface at constant temperature. However, when the crystal is heated the polarization changes resulting in a potential difference between the opposing surfaces of the crystal and results in the pyroelectric effect (Parker, 1983, 886).

Piezoelectric ceramics are manufactured by a process known as poling (figure 3). Above a critical temperature known as the *Curie point*, the ceramic crystal has a cubic symmetry containing no dipole moment. Below the Curie point the crystal structure changes to a tetragonal or rhombohedral symmetry resulting in a dipole moment. By subjecting the ceramic to an electric field as it passes through the Curie point, it is possible to polarize the crystal lattice and maintain the polarization after the ceramic is removed from the field.

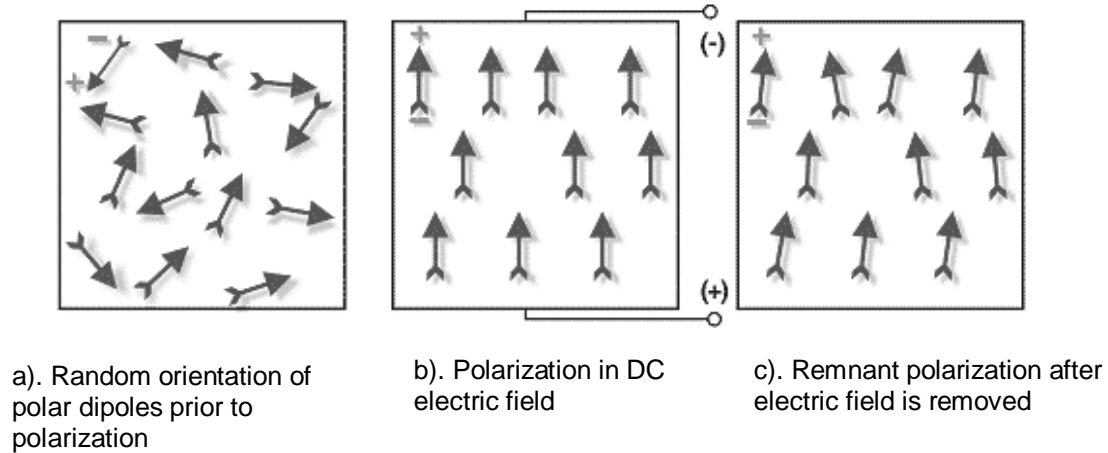


Figure 3. Polarizing (poling) a piezoelectric ceramic (Piezoelectricity, 2004)

Lead metaniobate is a good piezoelectric material for performing acoustic emission sensing. Besides being inherently rigid, it also has a low mechanical quality factor (Q_m), a high curie temperature, and a very good electromechanical coupling coefficient (k). A low Q_m indicates its usefulness as a wide bandwidth sensor and also indicates it has very good frequency resolution. Curie temperature indicates where the material's ferroelectric nature will begin to break down. The curie temperature for lead metaniobate is about 450° C, which means it can be used at very high temperatures without experiencing material failure (Lead Metaniobate, 6 Nov 2003; Piezoelectric Ceramic, 4 Nov 2003).

Piezoelectric physical properties are described by constants which contain information relating the direction of applied mechanical or electrical force and the directions perpendicular to that force. Each constant has two subscripts which indicate the direction of the two related properties (figure 4).

The piezoelectric charge constant, d , represents the degree of polarization generated per unit of mechanical stress applied. The first subscript of d represents the direction of polarization generated while the second subscript indicates the axis of the applied stress. For instance, d_{33} indicates an induced polarization in direction 3 per unit stress applied in direction 3. The strain induced in the piezoelectric material by an applied electric field is the product of the electric field and d .

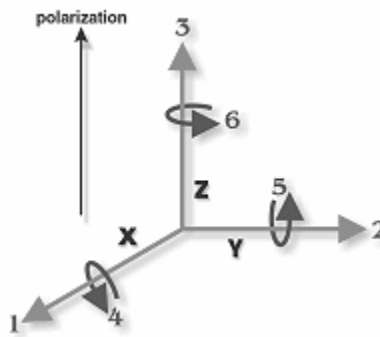


Figure 4. Direction of forces affecting a piezoelectric element (Piezoelectricity, 2004)

The piezoelectric voltage constant, g , is the electric field generated by the piezoelectric material per unit of mechanical stress applied. The first subscript of g represents the direction of the electric field generated while the second subscript indicates the axis of the applied stress. The strength of the induced electric field in the piezoelectric material is the product of the applied stress and the value of g .

The electromechanical coupling factor, k , indicates how effective the piezoelectric material converts mechanical energy to electrical energy or vice versa. The first subscript indicates along which axis an electrode is applied. The second subscript indicates the

axis in which mechanical energy is developed. Table 1 lists the values of the piezoelectric constants for the lead metaniobate ceramic used in the construction of the transducers used in this experiment (Piezoelectric Ceramic, 2003).

Table 1. Lead Metaniobate Physical/Electrical Properties

k_{31}	Transverse Coupling Coefficient	< .1
k_{15}	Shear Coupling Coefficient	.275
d_{33}	Piezoelectric Strain Constant ($\times 10^{-12}$ Coul/Newton)	85
d_{31}	Piezoelectric Strain Constant ($\times 10^{-12}$ Coul/Newton)	-15
d_{15}	Piezoelectric Strain Constant ($\times 10^{-12}$ Coul/Newton)	105
g_{33}	Piezoelectric Voltage Constant ($\times 10^{-3}$ Voltmeter/Newton)	32
g_{31}	Piezoelectric Voltage Constant ($\times 10^{-3}$ Voltmeter/Newton)	-7
g_{15}	Piezoelectric Voltage Constant ($\times 10^{-3}$ Voltmeter/Newton)	31
Q_M	Mechanical Q (Thickness)	< 15

Another quality of lead metaniobate that is attractive is its lead content. Lead has a high atomic number (82) which makes it more resistant to displacement. The energy that a neutron is able to transfer to a nucleus during an elastic collision is governed by the relationship (Turner, 1995, 213):

$$Q_{\max} = \frac{4mME_n}{(M + m)^2} \quad (1)$$

where m is the nucleus mass, M is the neutron mass, and E_n is the kinetic energy of neutron. It is apparent from equation (1) that as the neutron collides with an increasingly larger nucleus, it is able to transfer a smaller fraction of its available energy. Less energy transfer should reduce the degree of displacement damage to the crystal lattice of the piezoelectric material and enhance the survivability of the transducer.

Mechanics Study

Transducers.

When a force is applied to a piezoelectric crystal, a potential difference develops across the crystal that is proportional to the applied force. Piezoelectric sensors differ from static-force sensors, such as a strain gage, because the electric signal generated by the piezoelectric crystal is transient. This makes piezoelectric sensors unsuitable for measuring static forces but very useful for dynamic forces such as shockwaves or vibrations.

Some desirable aspects of piezoelectric sensors include their rugged construction, small size, self-generated signal, and high response speed. They are capable of detecting pressure events on the order of a millionth of a second. The radiation pulse width of the ACRR lasts seven milliseconds. Any shockwave resulting from the pulse would easily fall within the transducers response range. Unfortunately, piezoelectric sensors are also sensitive to temperature changes and require special cables and amplification. Table 2 compares piezoelectric transducer specifications with some other types of sensors.

Table 2. Typical Sensor Specifications (Holbert, short course, 2004)

	Accelerometer Range	Pressure Range	Bandwidth	Size
Variable Capacitance	2 g – 100 g	3 psi – 200 psi		
Force Rebalance	0.5 g – 125 g		Dependent on low pass filter	
Piezoelectric	0 g – 50,000 g	0 psi – 150,000 psi	20 Hz – 8 MHz	0.4 – 32 gm
Piezoresistive	2,000 g – 200,000 g	0 psi – 30,000 psi	150 kHz – 1300 kHz	0.1 – 50 gm

Piezoelectric transducers translate acoustic wave energy propagating in a material to an electrical signal. Generally, the electric potential will be proportional to the wave intensity which allows calibration of the transducer for use in measuring force.

Alternatively, the transducer can also be used to convert electric potential into mechanical vibration. By applying an alternating potential across the material, the molecular dipoles align themselves, causing the material to expand or constrict. This is known as electrostriction.

In a typical transducer, the transduction element is usually composed of a stack of piezoelectric wafers positioned such that when a force is applied the resulting dipoles in each wafer will be end to end and the total voltage produced will be the sum of each individual wafer. The thickness of the element determines the range of frequency sensitivity of the transducer. A wafer will vibrate from a wavelength that is twice its thickness. Therefore, the higher the desired frequency of detection or transmission, the thinner the piezoelectric wafers (Khazan, Piezoelectric Force Transducer, 5 Nov 03; Piezoelectric Transducers, 5 Nov 03).

A type of piezoelectric transducer of particular interest in this research is the acoustic emission (AE) transducer. Acoustic emission testing is used to detect and locate crack or leaks in pressurized systems. Generally, the systems are composed of metal but the technique can also be used with glass and carbon fiber.

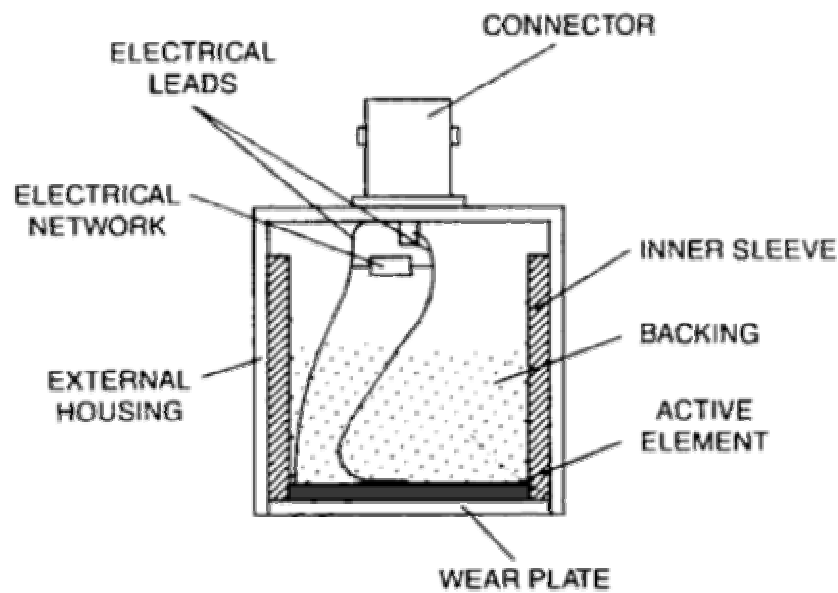


Figure 5. Piezoelectric transducer (Piezoelectric Transducers, 2003)

When stress is applied to a metal structure, it will deform to some extent. As stress increases, the metal will reach a point where permanent microscopic deformation starts to occur. At this point the metal will release stored energy in the form of elastic acoustic waves. This process is called ‘Acoustic Emission’ (AE) and can be detected by broad band piezoelectric transducers mounted on the surface of the material. Every metal has a characteristic AE frequency which can be used as a means for identification. By

using multiple sensors at various locations, it is also possible to determine the location of an AE source by using frequency time of arrival and mathematical triangulation techniques. Normal frequencies for AE range from 30 kHz to 30 MHz (Acoustic Emission, 2004).

Acoustic emission transducers are designed to be able to detect a wide bandwidth of frequencies with good resolution, which is why lead metaniobate is a good choice as a piezoelectric ceramic for AE detection. It has a low Q_m indicating its usefulness as a wide bandwidth sensor and also indicating it has very good frequency resolution.

Los Alamos has been using the B1025 AE piezoelectric transducer made by Digital Wave Corporation for the research they have been conducting. They have already conducted several pulse experiments in the ACRR using these transducers to measure the shock induced into a sealed canister, locate acoustic emission sources, and identify the composition of the source. The interpretation of the results is contingent on the effect of the radiation pulse on the transducer itself. The B1025 AE transducer will therefore be the sensor used to conduct this experiment in determining the damage effects of neutron radiation.

Table 3. B1025 Transducer Specifications

Frequency Bandwidth	50 kHz – 2 MHz
Temperature Range	-50°C – 100°C
Dimensions	0.365" OD x 0.5" H
Piezoelectric Crystal	0.25" diameter

Acoustics.

Acoustic waves traveling in a hollow tube can be described as guided waves and the hollow tube can also be considered a waveguide. It is also possible to use a solid metal rod to propagate acoustic longitudinal waves. This is the type of waveguide that is of interest for conducting this experiment. By attaching an acoustic pulser at one end of the rod and coupling the transducers to the other end, the response to the acoustic pulse can be measured after propagation through the waveguide. Using this technique, it is possible to transmit a controlled signal of known frequency to the transducers and measure their response while they are being actively irradiated. Neutron damage effects can be observed and measured in situ.

The type of material used as a waveguide can have an impact on the frequencies that are transmitted or the quality of wave propagation. To determine whether a particular frequency can be transmitted, it is necessary to consider the longitudinal wave equation:

$$\frac{\partial^2 \xi}{\partial t^2} = c^2 \frac{\partial^2 \xi}{\partial x^2} \quad \text{where} \quad c^2 = \frac{Y}{\rho} \quad (2)$$

where ξ represents longitudinal displacement, c is the wave propagation velocity in the media, Y represents Young's modulus, and ρ is the media density. Given the initial conditions that $\xi = 0$ and $x = l$, the solution to this equation is:

$$f_n = \frac{nc}{2l} \quad \text{where} \quad n = 1, 2, 3... \quad (3)$$

where f is the frequency, c is the wave propagation velocity, l represents the length of the waveguide, and n indicates the mode of vibration with $n = 1$ being the fundamental mode (Kinsler, Fundamentals of Acoustics, 59).

Using the solution to the wave equation, several materials were evaluated to determine what frequency range each would accommodate. Using a length of 72 inches, which represents the distance of the Ohio State University Reactor neutron beam port, and the physical constants for each material, the fundamental modes were calculated and are displayed in table 4 for comparison. The materials all performed equally with the fundamental mode being about 1.4 kHz. Since the fundamental frequency is well below the operational range of the B1025 AE transducer, which is rated from 50 kHz to 2 MHz, all of these materials are still acceptable for use in constructing a waveguide.

Table 4. Fundamental frequency for various metals

	Density (ρ) (g/cc)	Young's Modulus (Y) (millions of psi)	Fundamental Frequency
Aluminum	2.7	10	1.38 kHz
Carbon Steel	7.86	30	1.4 kHz
Stainless Steel	8.0	28	1.34 kHz
Titanium	4.5	16	1.35 kHz

The second consideration for material selection is the quality of wave propagation. To minimize loss of signal, the type of material selected should have a low degree of wave attenuation. The intensity of sound transmitted through a medium can be determined by the relationship:

$$I = I_o e^{-\alpha r} \quad (4)$$

where I_o is the initial intensity, α is the intensity absorption coefficient, and r is the distance from the sound impulse source.

In gases and liquids it is possible to determine the intensity absorption coefficient and use it in a great number of practical applications. The theory of sound attenuation in solids however is complicated by many mechanisms to include: heat conductivity, scattering from grain boundaries, magnetic domain losses, interstitial diffusion of atoms, and dislocation relaxation processes in metals (Parker, Acoustics Source Book, 38).

To determine the most suitable material for use as a wave guide, a more pragmatic approach was used. Rods of various materials acceptable from a radiation standpoint (see the discussion on *activation* in the radiation study) will be tested on the bench and the results will be compared to determine which material transmits the maximum wave amplitude for a constant initial pulse. By selecting the material with minimum wave attenuation, signal to noise ratio will be enhanced.

An example of an attenuation bench test is illustrated in figure 6. In this case, a steel bar measuring two feet in length is connected with a signal transmitter at one end and a receiving transducer at the other. A one volt sinusoidal frequency sweep is transmitted through the bar and the received pulse (top) is compared to the transmitted pulse (bottom).

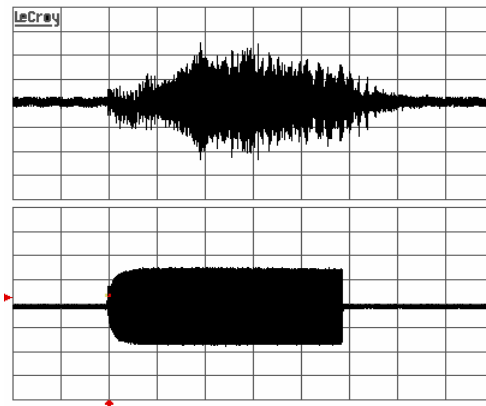


Figure 6. Acoustic source signal (bottom) and transducer response (top)

Thermal Effects.

Materials that are exposed to a radiation field will absorb energy from interactions with the radiation at the atomic and nuclear level. Some fraction of this deposited energy will be transformed into heat. It is therefore reasonable to assume there will be thermal heating in the materials during the experiment resulting in expansion and contraction between the transducers and the waveguide.

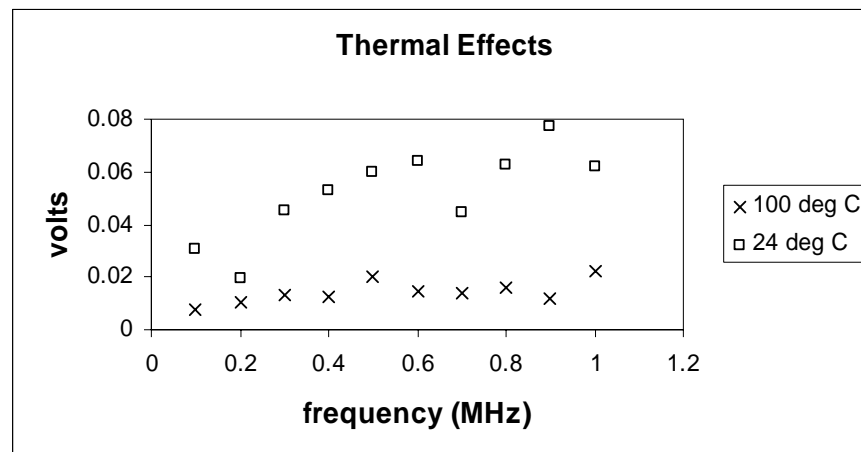


Figure 7. Thermal effect on transducer response

To determine the effects of thermal expansion, it is necessary to characterize the system at various temperatures to observe how expansion and contraction affect the apparatus. Figure 7 illustrates a characterization of the transducer response to a series of acoustic pulses transmitted through the waveguide at room temperature and at 100° C.

Coupling.

A couplant is a material that facilitates the transmission of acoustic energy between a transducer and an object. Couplant is used because there is an acoustic impedance mismatch between air and solids which results in a large percentage of acoustic energy being reflected instead of transmitted into a test material. Couplant displaces the air and makes it possible to get more sound energy into the test material so that a greater acoustic signal can be generated or received. A typical couplant in AE transducer work is silicon vacuum grease, but even a small amount of petroleum jelly will work.

Although using a couplant is standard procedure when working with transducers, its use will not be possible during this experiment due to the adverse effect that radiation will have on it. Silicon lubricants suffer a 25% viscosity change at 5×10^8 rads and organic lubricants are subject to gas evolution and viscosity change which eventually results in polymerization into a solid form (Etherington, Nuclear Engineering Handbook, 10-134, 10-146). Because no couplant can be used, acoustic signal transfer to the transducers will be considerably diminished.

It is possible to enhance signal transmission between the waveguide and the transducers by having the transducer/waveguide contact site polished to a very smooth

finish. Applying a large, constant pressure on the transducers when seating them in contact with the waveguide will ensure coupling does not change during handling of the equipment.

Radiation Study

Dose Determination.

A fundamental consideration in a radiation study is the determination of the dose rate and the total dose. Dose can be described as the amount of energy that is deposited in a small volume of material by the radiation emanating from a source. Mathematically, it is not difficult to define and calculate radiation dose. From a practical perspective though, it is a very difficult task because it is not possible to directly measure the energy deposited in a volume of matter by radiation (Kerris, 1992, I-2).

Dose rate can be defined as:

$$Dose\ Rate = \psi(E) \cdot \frac{\Sigma(E)}{\rho} \quad (5)$$

where ψ is the energy dependant flux, Σ is the energy dependant macroscopic cross section, and ρ is the material density. As a spectrum of radiation energies are introduced, it is necessary to modify this relationship to

$$Total\ Dose\ Rate = \int_0^{E_{max}} \psi(E) \cdot \left(\frac{\Sigma(E)}{\rho} \right) dE \quad (6)$$

which will take into account the changes in flux and cross section as energy varies. To make equation 6 practical to use, it can be approximated by a summation of group energy dose rates as shown in equation 7.

$$Total\ Dose\ Rate = \sum_{E=1}^{E_{max}} \psi(E) \cdot \left(\frac{\Sigma(E)}{\rho} \right) \cdot E \quad (7)$$

The maximum energy that a neutron is able to transfer to a nucleus during an elastic collision is governed by the relationship given in equation 1.

$$Q_{max} = \frac{4mME_n}{(M + m)^2} \quad (1)$$

Every neutron collision having energy E_n will not result in maximum energy transfer however, so an average energy transfer (Q_{ave}) is a more appropriate term for use in determining neutron dose. A rule of thumb for neutron scattering is that $Q_{ave} = \frac{1}{2} Q_{max}$ and is exact for isotropic scattering in a center-of-mass system (Turner, 1995, 218).

Making this substitution into equation 7 gives,

$$Total\ Dose\ Rate = \sum_{E=1}^{E_{max}} \psi(E) \cdot \left(\frac{\Sigma(E)}{\rho} \right) \cdot \frac{Q_{max}(E)}{2}. \quad (8)$$

Using equation 8, it is possible to calculate the rate at which energy is being deposited in a material during irradiation given a neutron group energy spectrum and an energy dependant cross section for the material.

Neutron cross sections are not always available for every material of interest in dose calculations. After a thorough search of available databases, no information on cross sections for lead metaniobate could be found. However, the cross section information for each of the elements which make up lead metaniobate ($PbNb_2O_6$) is

available. A closer inspection of the macroscopic cross section provides a means to use the individual element cross sections to determine the total dose rate in lead metaniobate.

The macroscopic cross section (Σ) is related to the microscopic cross section (μ):

$$\Sigma = \frac{\mu \cdot N_A \cdot \rho}{GAW} \quad (9)$$

where N_A is the number of atoms per mole (Avogadro's number), ρ is the density of the element of interest, and GAW is the gram atomic weight or the equivalent weight of the element per mole. Since the ratio of the elements per unit weight of lead metaniobate (PbNb_2O_6) is easily calculated, the density of each element can be found (Appendix C). Now it is possible to calculate the macroscopic cross section for each element allowing an individual element dose rate calculation to be performed. The total dose rate will be the sum of the individual dose rates for lead, niobium, and oxygen.

The total dose is found by integrating the dose rate with respect to time. If the dose rate remains constant, then multiplying by the time of exposure will produce the total dose (Appendix D).

Damage Mechanisms.

The experiment will be conducted in an environment which is predominantly gamma and neutron radiation. The primary effect of gamma radiation is ionization damage while neutrons will primarily produce displacement damage.

Gamma radiation is electrically neutral but will interact with atoms through the photoelectric effect, Compton scattering, and pair production. The first two interactions result in ionization and energetic secondary electrons. Pair production produces a

positron-electron pair. The photoelectric effect predominates at low photon energies and high atomic numbers (Z). As photon energy increases, Compton scattering begins to dominate over the photoelectric effect. Pair production has a threshold energy of 1.022 MeV and increases in probability as Z increases (Srour, 1988, IV-4).

The energetic secondary electrons that result from the photoelectric effect and Compton scattering continue to produce more secondary electrons by Rutherford scattering. This process results in the creation of electron/hole pairs which can act as charge carriers.

Ionizing radiation can affect the characteristics of an insulator by creating leakage current. Insulators contain charge trapping centers in which radiation-induced charge carriers can be trapped for long periods of time. As trapped charge accumulates, internal space-charge electric fields are generated which can change the insulators electrical characteristics. The creation of charge carriers in the insulator can cause an increase in conductivity by several orders of magnitude, even in a low flux radiation field (Huth, page 2). It is possible that this effect could reduce the potential difference generated by the piezoelectric transducer in response to an acoustic pulse.

Neutron radiation is electrically neutral and does not interact with electrons. Instead, neutrons pass through the electron cloud of an atom and interact directly with the nucleus resulting in elastic scattering, inelastic scattering, and transmutation.

In elastic scattering, the neutron collides with a nucleus and transfers a fraction of its energy to the atom. This can dislodge the atom (figure 8) from the material's crystal

lattice and is referred to as “displacement damage”. The atoms displacement may create a “Frenkel pair” which consists of a vacancy and an interstitial atom.

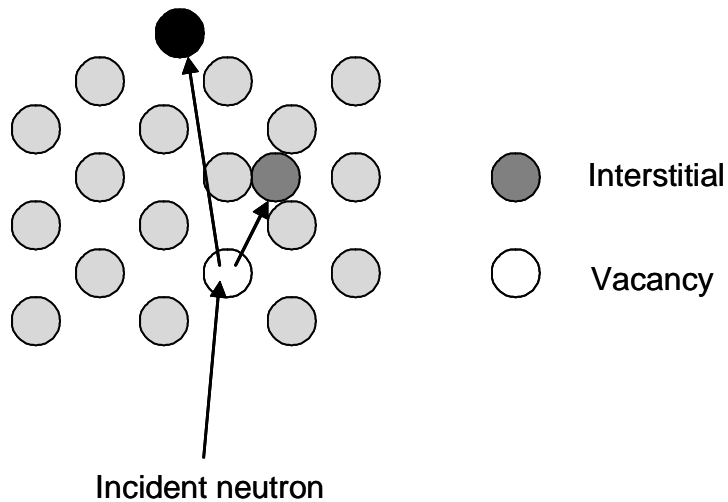


Figure 8. Displacement damage in crystal lattice

Inelastic scattering involves capture of the incident neutron by the atom nucleus followed by subsequent emission at a lower energy. The difference in energy between the incident and emitted neutron remains in the atoms nucleus leaving it in an excited state. The nucleus will eventually return to its ground state by emitting a gamma ray. Inelastic scattering can also cause displacement damage.

Transmutation, also known as “activation”, involves capture of the neutron in the nucleus and subsequent emission of a different particle, such as an alpha or beta particle. The emission of a different particle transmutes the atom to a different element.

Activation.

Neutron activation is an effect that must be considered in the design of this experiment. Radioactivity can be induced by the capture of a neutron in a sample atom's nucleus. This event causes a transmutation in the nucleus of the sample atom and often results in an unstable isotope which will eventually decay with a characteristic half-life and emit radiation. Two activation products that will occur during this experiment are ^{28}Al and ^{55}Fe (aluminum and iron are used to manufacture the transducer) which have half-lives of 2.25 minutes and 2.73 years respectively. Excessive radioactivity in a material will result in it becoming a biological hazard and must be avoided to the extent that personnel involved in its handling may not exceed exposure standards prescribed in 10 CFR Part 20.101.

Materials subjected to the reactor environment must be given careful consideration. Material attributes that will help mitigate the radiation hazard include a short half-life, small physical quantity, and small neutron cross section. Although this precludes use of the majority of wave guide material, there are still a few viable candidates, which include: aluminum, titanium, Lucite, glass, quartz, silicon, and some ceramics. Materials with a short half-life will decay below hazardous levels in a short enough time to be practical, assuming they decay to a stable isotope. For instance, aluminum-28 has a two minute fifteen second half-life and therefore will decay to safe levels (secular equilibrium) after seven half-lives, which is less than 16 minutes (Turner, 1995, 90).

Noise Generation.

Ionizing radiation can generate noise in experiments that involve electronic devices. Effects of ionization that can lead to noise include leakage current, and Compton current. The most important sources of noise occur where the signal originates and is weakest in strength. Noise generated at this point will go through the same amplification process as the signal.

Ionizing radiation can cause leakage current in insulating materials used in a device. Fluctuations in leakage current inside of the transducer would result in noise generation at the signal origin. The noise would then be amplified along with the signal resulting in increased measurement variance (Knoll, 2000, 629).

A Compton current is generated by streaming ionizing radiation. There is a net direction of the Compton electrons resulting in a current. Streaming radiation will primarily be in the neutron port where the coaxial cables for the transducers will be located. Since the cable consists of a parallel positive and negative lead, there should be no net effect on the transmitted signal. Also, since piezoelectric transducers measure force by the generation of a potential difference, there is no current involved and so Compton current should have no effect.

Signal noise may or may not be a problem. If the noise becomes excessive, the response signals may be lost or rendered so weak that the level of error is unacceptable. To prevent this from occurring, several precautions can be taken. Selection of low noise, radiation resistant insulated cables will help minimize the contribution of noise due to gamma and charged particle interactions in the cable. Also, the best precaution for

ensuring that reliable data is collected is to have sufficient signal strength to overcome the noise introduced by radiation. This can be achieved through signal amplification.

III. Experimental Design

Equipment and Test Station Configuration

The design of the experiment begins with setting up the required equipment. The configuration is illustrated on figure 9. An HP 33120A Arbitrary Waveform Generator provides a discrete frequency acoustic pulse to an Ultratran LC50-2 piezoelectric transducer (pulser), which is used to generate an acoustic pulse by taking advantage of the electrostrictive property of piezoelectric materials.

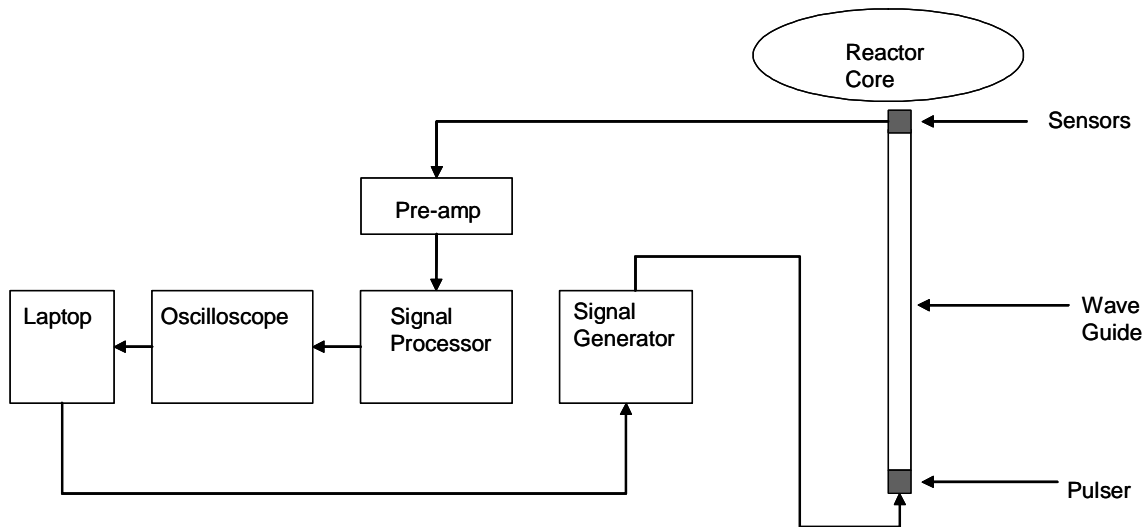


Figure 9. Experiment test station configuration

The pulser is coupled to the waveguide outside of the nuclear reactor. This allows the pulser to generate an acoustic pulse for propagation to the interior of the reactor without being exposed to the radiation field and causing radiation damage. Three B1025 Digital Wave transducers, which are coupled to the reactor end of the waveguide, will

generate a response signal to the acoustic pulse. The response signal will travel back to the test station through RG-174 low noise coaxial cable. Figure 10 shows the relative size of the Ultran pulser (left) and the Digital Wave transducer (right).

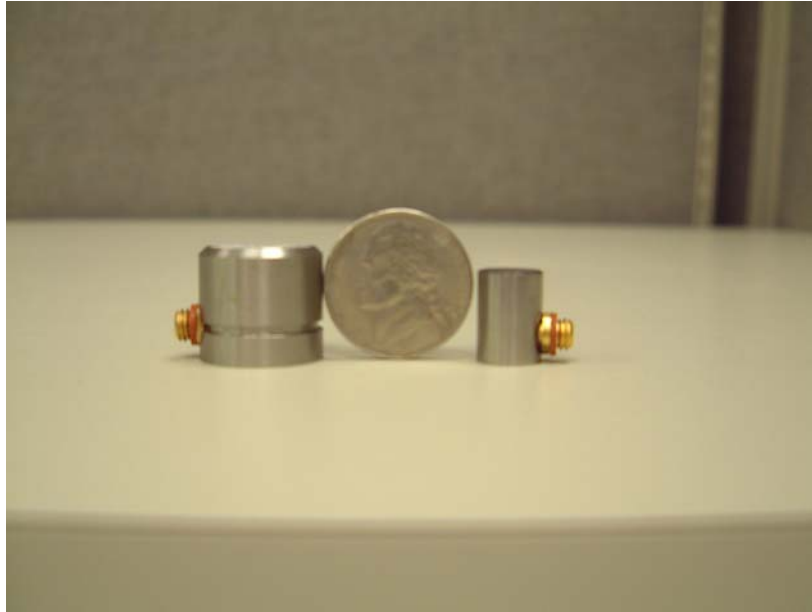


Figure 10. Relative size of pulser (left) and transducer (right)

It may be informative at this point to see how the Digital Wave transducer is internally constructed. Figure 11 gives a cross sectional view of the transducer. At the bottom is a thin, light grey strip which is the lead metaniobate piezoelectric ceramic. The large, dark grey mass directly above the ceramic is a tungsten backing. The white material above the tungsten is an epoxy which binds the backing and prevents it from moving. An electrical wire, which has been cut, makes contact with the top of the piezoelectric. The bottom of the ceramic is in contact with the transducer casing, thereby completing the electrical circuit.

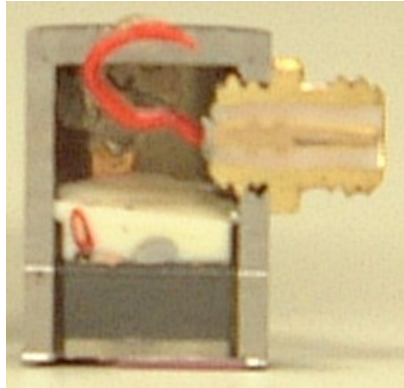


Figure 11. Cross section of B1025 AE transducer

The signal is then fed into a Digital Wave PA 2040A pre-amp to increase signal strength and is subsequently transmitted to a Digital Wave FTM 4000 signal processor. The signal processor provides frequency filters, gain control, trigger control, amplification, and power for the pre-amplifiers.

The processed signal pulse is captured by a LeCroy Waverunner LT584M 4-channel digital storage oscilloscope. Three channels handle the data acquisition for the individual transducers inside the reactor during testing. The fourth channel is dedicated to monitoring the source signal and also serves as the trigger for capturing the signal from the transducers in the reactor. The oscilloscope is able to store the captured waveforms digitally and transfer the information to a laptop computer for processing. It also has the capability to transfer screen picture images of the captured waveforms to computer which allows much faster data processing decisions to be made by the operator.

Experimental control and data management is provided by a Dell Precision laptop computer. It is equipped with an IEEE 488 interface for control of the signal generator, the digital oscilloscope, and data transfer.

Waveguide Construction

Several materials were tested for suitability as a waveguide. Factors which influenced the selection included cost, ease of machining, activation half-life, signal attenuation and availability. Materials that were tested included titanium, carbon steel, stainless steel, and several grades of aluminum. Graphite, Pyrex glass, and Lucite were viable candidates based on cost, activation, and signal propagation. Unfortunately, either ease of machining or availability eliminated them from consideration prior to testing. All of the materials tested performed acceptably with regard to signal attenuation except some of the softer grades of aluminum.

Carbon steel and stainless steel are very hard metals and are difficult to machine. They also have very long lived activation products. Natural iron contains 6% of the isotope ^{54}Fe . Neutron activation of this isotope will produce ^{55}Fe which has a half-life of 2.7 years. These materials were not very favorable for use in the experiment.

Titanium has very attractive properties as a waveguide. Primarily, it has minimal activation problems. ^{50}Ti has a naturally occurring isotopic abundance of 5%. The activation product ^{51}Ti has only a 5.75 minute half-life. Unfortunately, titanium is very expensive and availability was very limited. Due to time and financial constraints it had to be eliminated.

Aluminum was chosen as the material to use for construction of the waveguide. 100% of aluminum occurs naturally as ^{27}Al . Neutron capture will produce ^{28}Al which has a half-life of only 2.25 minutes. Harder grades of aluminum performed well with respect to low signal attenuation. Aluminum is also reasonably priced, easily machined, and readily available. 20-24 T351 aircraft grade aluminum was selected for use in constructing a waveguide.

A 7 foot length by 1¼ inch diameter aluminum rod was selected as a wave guide to the B1025 sensors that are to be inserted next to the core of the OSURR. The Ultran LC50-2 pulser will attach to one end of the wave guide and at the other end the three B1025 sensors will be secured to the waveguide by a 1¼ inch diameter by ¼ inch thick aluminum plate fastened to the waveguide with a steel bolt (figure 12).

The reactor portal at OSU that will be used for this experiment has a depth of approximately seven feet. The sensors to be tested must be inserted fully, if possible, in order to maximize the neutron fluence in the limited amount of time available. Eight feet of cable will be required to maintain connectivity with the sensors, which is a significant distance. It is not possible to pre-amplify the transducer signal during the first seven feet of transmission because the cable is in the neutron port where streaming radiation will interfere with signal amplification and could possibly damage the pre-amplifiers. Instead the experiment will rely on a strong source signal to overcome noise if it becomes a factor. The HP 33120A Signal Generator can drive a 10 volt peak-to-peak signal which should provide sufficient signal strength. The pulser is capable of being driven by

potentials of several hundred volts and an a/c amplifier could be inserted between the signal generator and the pulser if necessary.

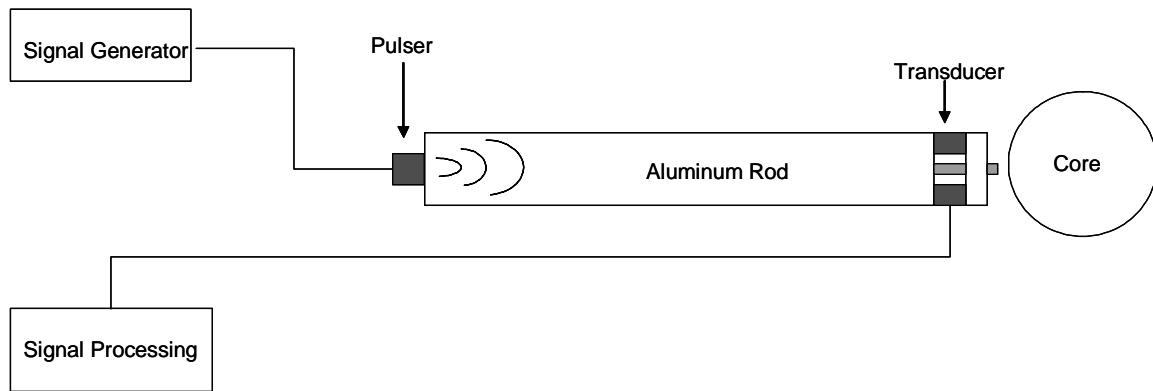


Figure 12. Wave guide apparatus

To place the transducers in the radiation field near the core, the neutron port will have to remain open because of the rigid nature of the waveguide. This presents a radiation hazard since the neutron portal is six inches in diameter and will allow streaming radiation to escape directly from the core. .

To attenuate the gamma radiation escaping from the portal, a combination of lead shielding and concrete bricks was used. To absorb thermal neutron radiation, cadmium foil was used. Cadmium is very effective for absorbing thermal neutrons, but there is also a significant fast neutron flux that must be thermalized in order to be absorbed by cadmium. To do this, a six foot long by six inch diameter low density polyethylene cylinder was machined to allow the aluminum waveguide bar to fit in the middle. The polyethylene was placed in the neutron port to fill the void space while the waveguide fit neatly in the center and extended into the reactor core.

Plastic molecules have a high density of hydrogen atoms, which have a nucleus consisting of one proton that is of equal mass to a neutron. Referring back to equation 1, the energy a neutron is able to transfer (Q_{\max}) to a nucleus during an elastic collision is governed by the relationship:

$$Q_{\max} = \frac{4mME_n}{(M + m)^2} \quad (1)$$

If the mass of the nucleus (m) is the same as that of the neutron (M) then it is possible for the neutron to transfer all of its energy to the nucleus, resulting in maximum neutron thermalization. Polyethylene should therefore be very effective at moderating the fast neutron flux

Data Sampling Method

The initial sampling method was to generate a sinusoidal wave which swept a continuous range of frequencies in approximately one second. The frequency of the sweep would vary linearly with time and therefore a particular frequency response could be determined and used for analysis and comparison.

An example of this technique is illustrated in figure 13 with the bottom waveform representing the source signal generated by the LC50-2 pulser and the upper waveform representing the response from the B1025. This particular example was performed with the pulser coupled directly to the transducer in a “face-to-face” geometry. The result is a response signal that is not as distorted or attenuated as it would be if the waveguide were placed between them.

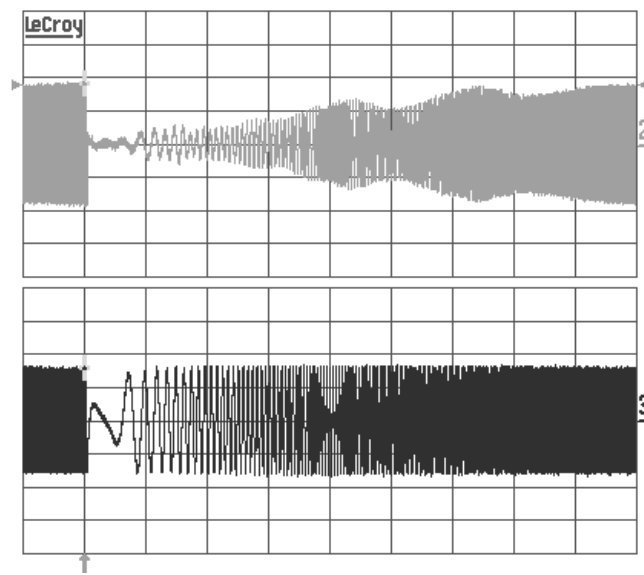


Figure 13. Frequency sweep from 1 kHz to 500 kHz with source signal (bottom)
compared to response signal (top)

As routines for processing the raw data were developed, problems with the frequency sweep sampling technique became apparent. Attempts to compare separate sample response values at a specific frequency resulted in standard deviations that were very often much greater than the mean value measured. The problem was caused by a variable time delay in the trigger which resulted in a frequency shift for each sample. Consultation with the oscilloscope manufacturer was not successful in solving this problem.

To overcome this problem, discrete frequency pulses were programmed into the signal generator for response analysis. Ten frequencies were selected beginning with 100 kHz and ending at 1 MHz using increments of 100 kHz. The response waveforms from the B1025 sensors were very consistent. Figure 14 shows the response of three

transducers to a 600 kHz pulse. Channel 4 shows the source pulse generated by the LC50-2.

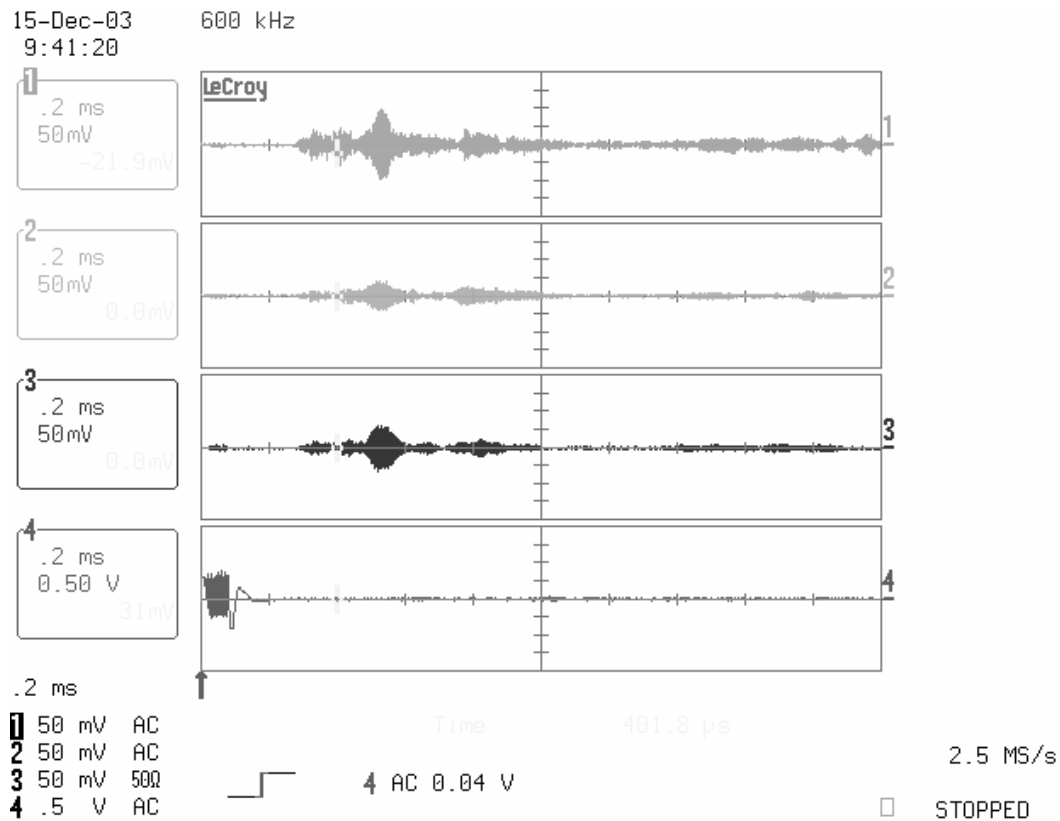


Figure 14. Transducer response to 600 kHz acoustic pulse

The signals captured on the display of the oscilloscope are also recorded internally as data files of the time varying voltage response and can be transferred to a computer for analysis. A 100 kHz data file is graphed in figure 15. This particular sample contains 5000 data points. Although it provides an interesting visual representation of the transducer's response, the data is not in a very useful format for analysis and comparison with other samples.

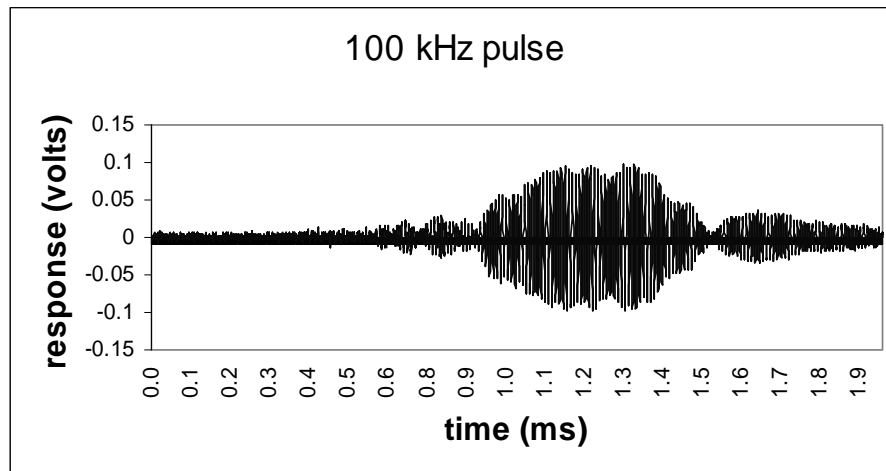


Figure 15. 100 kHz response data file

An investigation into the design of the digital oscilloscope produced a feature which allowed processing of the waveform to determine the maximum response measurement. The maximum measurement could then be stored and transferred to a computer. Using this feature, ten maximum responses were gathered for the ten sampling frequencies on all three transducers. One sampling cycle consisted of 300 acoustic pulse events and required approximately six minutes to complete. The mean value was determined at each frequency using the ten recorded max responses, and the standard deviation was calculated.

Statistical analysis of this sampling method (figure 16) resulted in very reproducible pulse height measurements. The standard deviation ranged between 3% and 8% of the mean value for all frequencies.

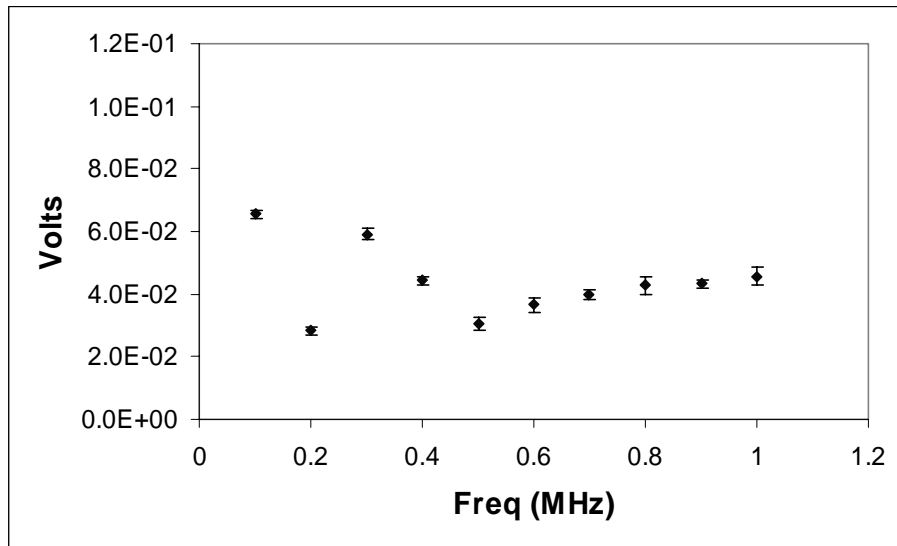


Figure 16. B1025 transducer response precision with 1 standard deviation error bars

Measurement System Characterization

After fabrication of the waveguide was complete, the measurement system was connected to the transducer/waveguide apparatus to begin characterization of the system in a radiation-free environment and to also characterize the effects of thermal heating.

Figures 17, 18, and 19 show how the pulser and transducers were connected to the waveguide for characterization measurements. The surface face at each end of the waveguide was machined and finished to a highly smooth surface to maximize acoustic coupling with the B1025. No couplant was used with the B1025 sensors because of the adverse effect that radiation will have on it. Characterization results are displayed in figure 20.

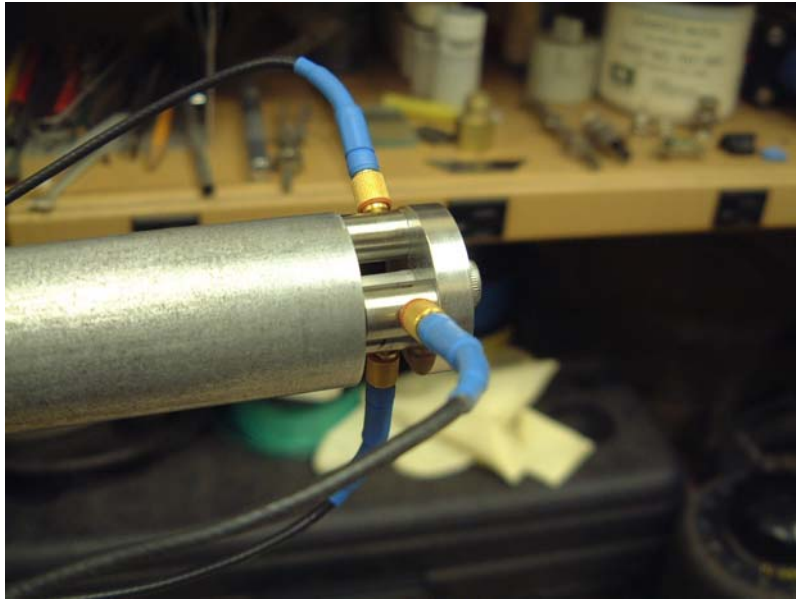


Figure 17. Waveguide and transducers



Figure 18. Waveguide and transducers

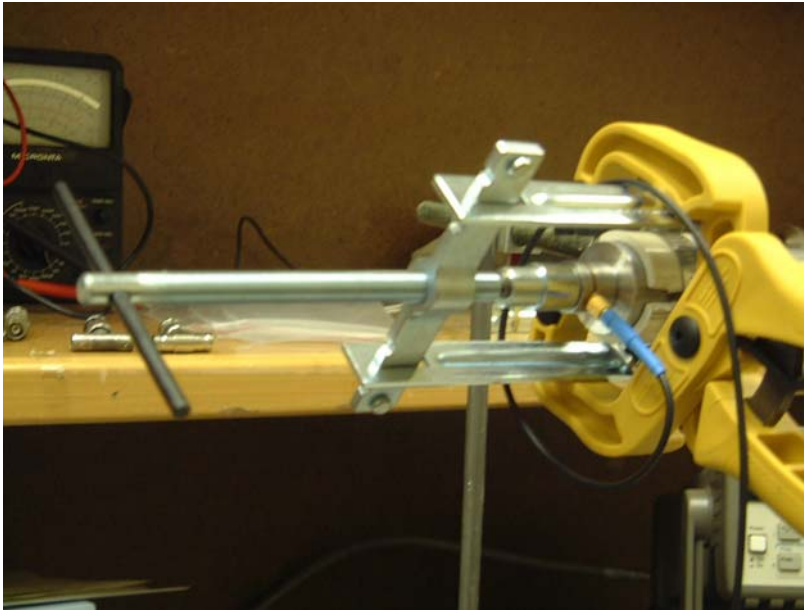


Figure 19. Pulser connection to waveguide

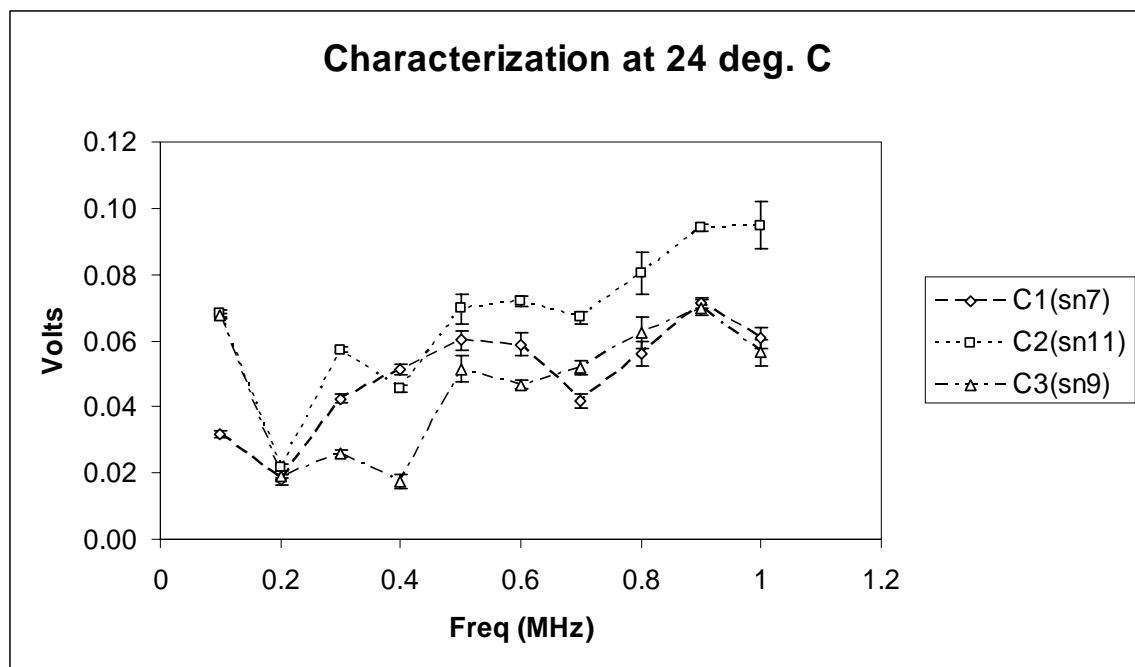


Figure 20. Bench characterization of transducers at 24°C

The characterization in figure 20 shows the response of three transducers to ten discrete frequency pulses transmitted through the waveguide. The error bars represent one standard deviation based on ten separate measurements for each frequency. Each individual measurement is the maximum potential generated by the transducer in response to the acoustic pulse generated at the pulser end of the waveguide.

The characterization shows that each transducer has a unique response profile. This is due to the manufacturing process, which is not precise enough to create transducers with consistently equal response. The most common variable causing variation in transducer response is the orientation of the crystal lattice in the ceramic element. The piezoelectric coefficients are defined with respect to the lattice cell orientation. If the lattice varies in the ceramic element or there are variations in the ceramic geometry during transducer construction, the response of the transducer will be affected.

To maximize acoustic signal transfer and propagation, silicon vacuum grease *was* used as a couplant between the pulser and the waveguide. It is important to emphasize that a couplant can be used because the pulser is **not** in the reactor. There will not be any damage to the pulser or any degradation to the couplant.

During irradiation, the transducers will increase in temperature due to absorbed dose. Response values may be affected due to pyroelectric effects in the lead metaniobate. Thermal expansion of materials could also alter the response by changing the static pressure on the piezoelectric element. Another characterization will be required to differentiate thermal effects from radiation damage effects.

It is possible to determine an upper and lower limit on the expected temperature range inside the neutron portal by determining the dose rate of the lead metaniobate and performing a radiative heat transfer analysis of the transducer/waveguide system.

The waveguide and transducer assembly is contained inside the neutron port which is a sealed aluminum housing surrounded by the reactor coolant pool. When the transducers are irradiated, they will heat the waveguide assembly by conduction. As the assembly increases in temperature, it will radiate heat to the surrounding air according to the radiation heat transfer equation:

$$q = \sigma \varepsilon A (T_w^4 - T_\infty^4) \quad (10)$$

where q is the rate of heat flow out of the system by radiation (J/s), σ is the Stefan-Boltzmann constant, ε is the emissivity of the surface (dimensionless), A is the surface area through which the heat flows (m^2), T_w is the absolute surface temperature (K), and T_∞ is the absolute ambient temperature (K) (Myers, 1987, 3).

Dose rate is calculated using equations 5, 6, and 7. The units of dose rate are joules per kilogram second (J/kg-s). The rate of heat generation in the system can be approximated if the dose rate is multiplied by the total mass of the lead metaniobate. Although some of the energy absorbed will be lost due to excited state gamma emissions and decay, the calculation will at least give the maximum rate of heat generation in the system.

The maximum expected temperature inside the neutron port is calculated by setting q in equation 9 equal to the rate of heat generation in the system and solving for the surface temperature T_w . To solve this equation, the emissivity of the aluminum

waveguide must be known. Emissivity for industrial grade aluminum varies between 0.1 and 0.3, depending on the extent of oxidation on the surface (Infrared Measurement, 2004). Appendix F contains the heat transfer calculations.

The maximum expected temperature was 31 degrees Celsius using an emissivity of 0.1 and a heat sink temperature of 30 degrees Celsius. The minimum expected temperature is the heat sink which is the cooling pool in this case. The temperature in the pool ranged from 30 to 35 degrees Celsius when the reactor power was at 450 kW.

To characterize the effects of thermal heating on the system, a chemical flask heating blanket was placed around the transducer end of the apparatus (figure 21) and the temperature was increased to the maximum rated operating range of the transducers, which is 100°C. Temperature was monitored with a standard thermometer inserted inside the blanket next to the transducers.



Figure 21. Thermal characterization

After reaching 100°C, the response of the transducers decreased considerably as shown in figure 22. As the temperature was reduced back to room temperature, the response did not recover and degradation continued to increase on several frequencies. Table 5 summarizes these findings and expresses the degradation as the average decrease for all ten frequencies sampled.

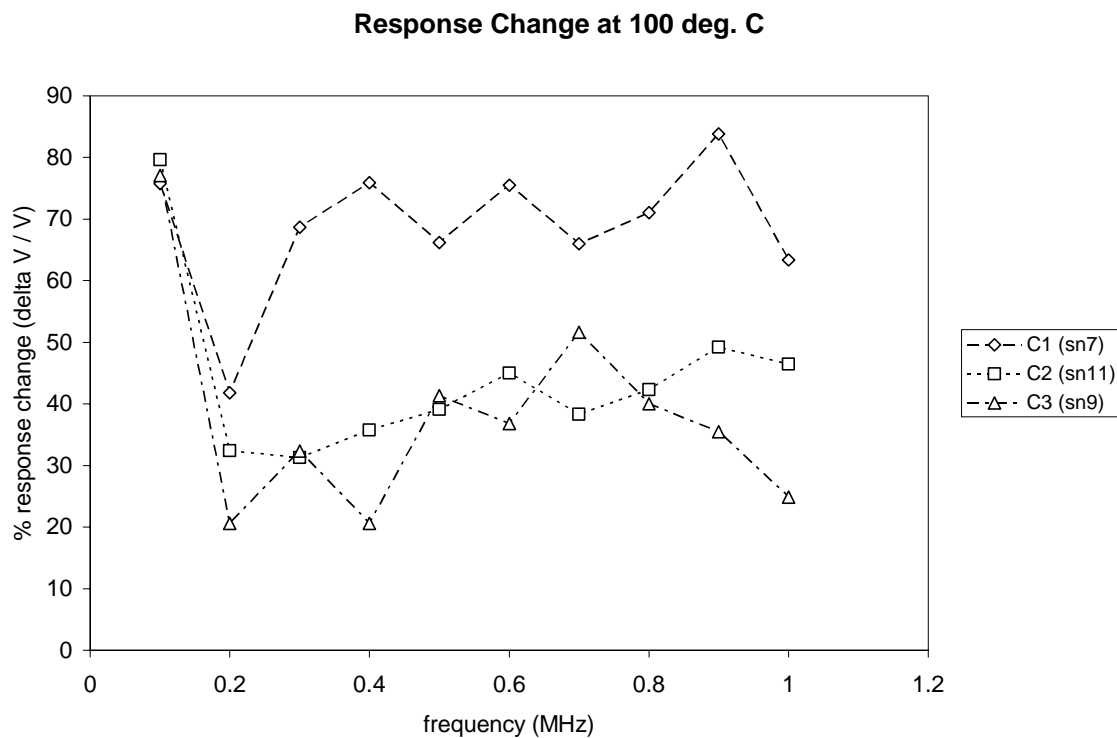


Figure 22. Transducer response change at 100°C

The thermal characterization was performed the day prior to the scheduled transport of the system to the OSU reactor. Due to time limitation, further investigation of the thermal effect on the transducer/waveguide system was postponed until after completion of the irradiation phase of the experiment.

Table 5. Average transducer response decrease

	Response decrease at 100°C	Response decrease after returning to 23°C
Channel 1 (sn 7)	69%	72%
Channel 2 (sn 11)	44%	55%
Channel 3 (sn 9)	38%	69%

Since response did not immediately recover with cooling, the apparent effect of thermal heating was permanent degradation of response. To ensure the best data acquisition during irradiation, the two transducers with a lower response (sn7 and sn9) were replaced with the last two remaining transducers. The irradiation at OSU was performed using transducers sn10, sn11, and sn12. Table 6 summarizes where each transducer was used during the execution of the experiment.

Table 6. Transducer tracking sheet

Serial Number	Characterization	Thermal Characterization	Irradiation	Internal Study	Thermal Effects
7	X	X		X	
9	X	X			X
10			X		
11	X	X	X		
12			X		

The internal study in table 6 consisted of cutting transducer sn7 in half in order to understand how it is constructed. Knowing how it is designed could help in interpreting the possible mechanisms of radiation damage to the transducers.

A second thermal experiment was performed on transducer serial number 9. It was brought to 100°C in two separate test sessions. During the first session, silicon vacuum grease was applied between the transducer and the waveguide. During the second session no couplant was used, as was the case during the initial test. The intent of this experiment was to determine whether thermal heating was causing response changes due to effects on the internal materials of the transducer or whether the response changes were due to external changes in coupling due to the expansion and contraction of the metal surfaces.

Couplant was used during the first session because during material expansion and contraction, voids may be created between the transducer and waveguide surfaces. This causes an acoustic impedance mismatch between the air-filled voids and the metal surfaces which results in a large percentage of acoustic energy being reflected instead of transmitted into the transducer. Couplant displaces the air and makes it possible to get more sound energy into the test material so that a greater acoustic signal can be received.

Examination of figure 23 indicates that when couplant is used, no significant change in signal response occurs.

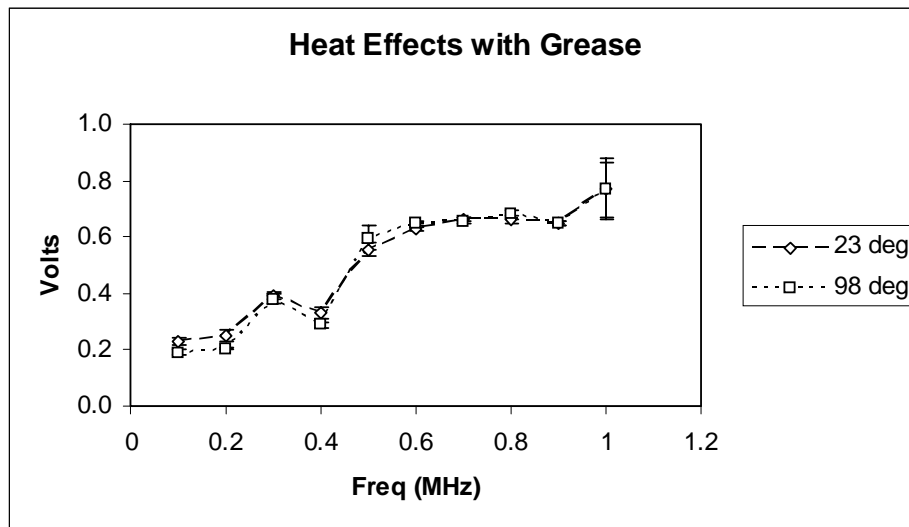


Figure 23. Thermal heating of transducer sn9 with couplant

When no couplant is used, the response signal varies significantly with increasing temperature as can be seen from figure 24.

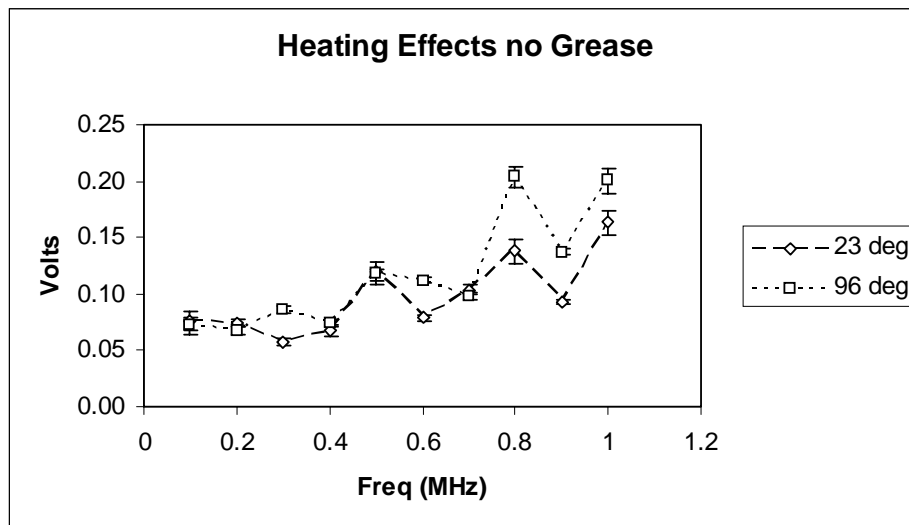


Figure 24. Thermal heating of transducer sn9 without couplant

An important detail in comparing figures 23 and 24 is that using couplant increases transducer response by a factor of about four.

Once the system had been characterized in the laboratory, a test run was performed with the waveguide and transducers inserted into the OSU reactor while it was shut down. Response measurements were recorded to establish an in situ characterization of the test station (figure 25). This information provides a baseline measurement for use in interpreting the experimental results.

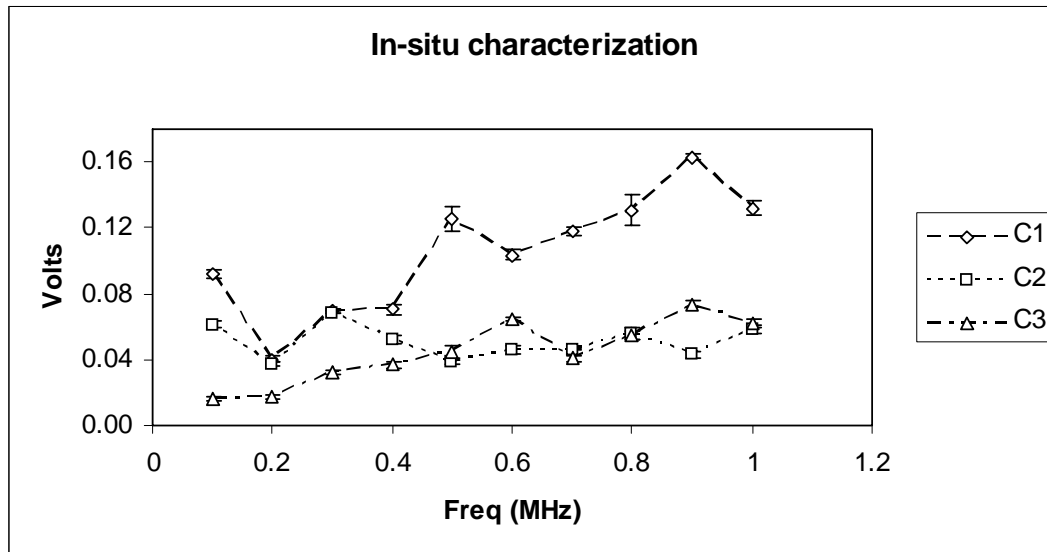


Figure 25. In situ characterization

Experimental Procedure

The transducer irradiation goal was to achieve $1 \times 10^{17} \text{ cm}^{-2}$ neutron fluence. A quick back-of-the-envelope calculation is useful to approximate how much time it would take to achieve that fluence. The OSU Reactor has a maximum power rating of 500 kW.

Running at 450 kW, the reactor has an approximate neutron flux of $2 \times 10^{12} \text{ cm}^{-2} \text{ s}^{-1}$. If the reactor were maintained at that power setting it would require 5×10^4 seconds, or about 14 hours of irradiation time to achieve the fluence goal. This is a minimum time calculation since the reactor will not always be running at 450 kW.

Initially, the reactor was powered up to only 50 kW in order to produce a neutron flux of approximately $10^{11} \text{ cm}^{-2} \text{ s}^{-1}$. This allowed a fluence of 10^{15} cm^{-2} to be achieved in 10^4 seconds, or 2.8 hours. This fluence is equivalent to a typical pulse in the ACRR at Sandia National Laboratory. Gradually approaching this fluence at 50 kW allowed more time to collect data in case the transducers should fail very early in the experiment.

During the first two days of irradiation, power was increased gradually to see how the transducers would respond. Since there was no published literature available on experiments of this nature, it was unknown how the transducers would be affected by either dose rate or total dose. The final two days were executed with the reactor running at full power. The entire irradiation experiment was completed over the course of four days.

When the reactor was shut down at close of business, sampling continued overnight to observe the recovery that occurred in the transducers. This was accomplished using computer controls to automate the data collection process. Although it would have been ideal to remove the waveguide from the neutron port to eliminate residual gamma radiation effects on the recovery behavior, activation of the entire test apparatus made it too radioactive to handle.

IV. Results and Analysis

Thermal Effects

The intent of this experiment was to determine whether thermal heating was causing response changes due to effects on the internal materials of the transducer or whether the response changes were due to external changes in coupling caused by the expansion and contraction of the metal surfaces.

Figure 26 indicates that thermal heating has little effect on the internal function of the transducer, at least at the temperatures observed. The results support the conclusion that thermal expansion of materials affects the coupling of the system if no couplant is applied.

Figure 27 shows that coupling is much worse between the transducers and the waveguide because the response magnitude is much smaller. It also illustrates a change in coupling with increased temperature. Both of these figures support the conclusion that it is possible the change in response of the transducers during the initial heat characterization was largely due to expansion of metal surfaces, which changed the coupling of the system.

It is also interesting to note that the heating response profile of transducer sn9 in figure 26 is nearly equivalent to its initial room temperature response profile in figure 20 while in figure 27 it is much lower. When the initial response profile was conducted, the finish on the surface of the waveguide was extremely smooth and no couplant was used. Figure 26 shows sn9 having nearly the same response as initially, but this time couplant

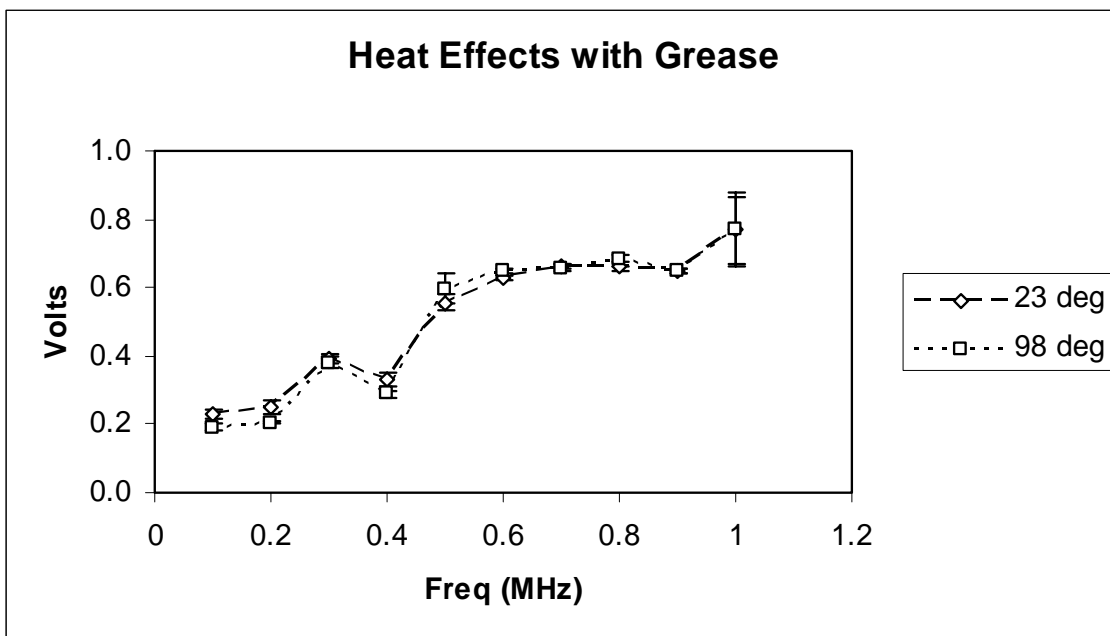


Figure 26. Thermal heating of transducer sn9 with couplant

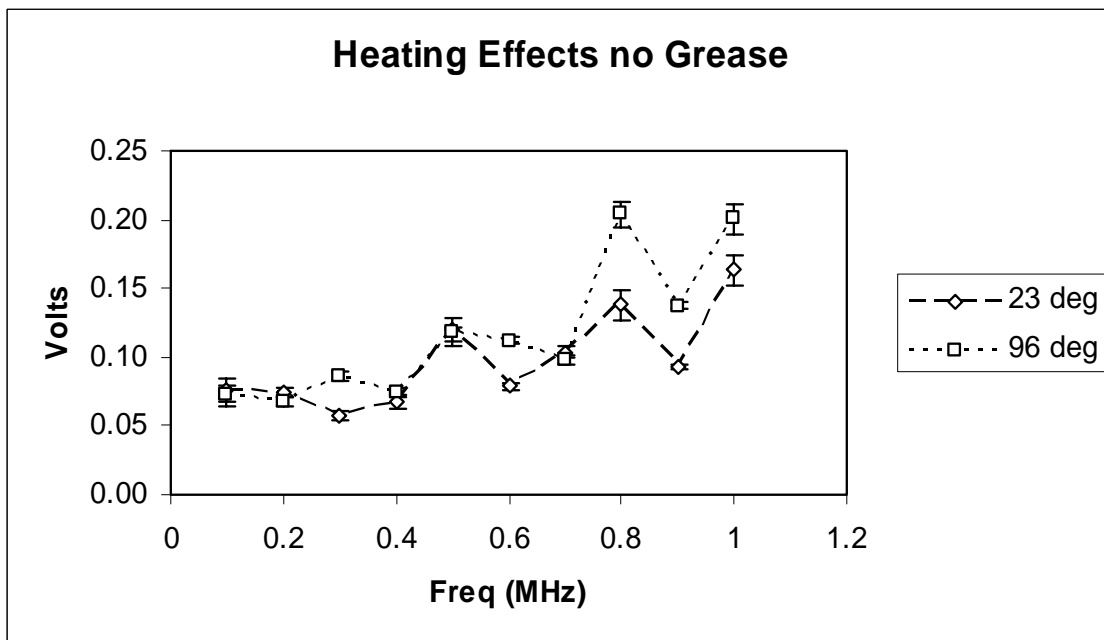


Figure 27. Thermal heating of transducer sn9 without couplant

is used. Two conclusions can be drawn from this observation. The first conclusion is that damage is occurring on the surface of the waveguide creating voids between the transducer and waveguide interface. This changes the impedance which results in reducing the transducer response. The damage is occurring from the numerous transducer changes between experiments and from expansion and contraction during the thermal heating experiments. The second conclusion is a consequence of the first. Since transducer sn9 appears to have a fully recovered response when couplant is used, it is apparent that no permanent damage was done to the transducers in the initial thermal effects characterization. Transducer response changes during heating were primarily due to changes in coupling.

Irradiation Results

Raw measurement text files were transferred to a spreadsheet and organized by transducer. Each point that is plotted on a graph represents a mean value of ten separate measurements. Sampling of the transducers always occurred simultaneously, therefore at any sample time each transducer will have the same radiation dose.

Figures 28 and 29 present the time changing response of the transducers at two frequencies. Appendix A contains similar data on the remaining eight frequencies that were studied.

The vertical lines through the graph delineate periods of irradiation from periods when the reactor was shut down. During the periods of reactor inactivity, the recovery behavior of the transducers can be seen. The abscissa represents the total number of hours transpired since initiation of the experiment. The ordinate contains the response,

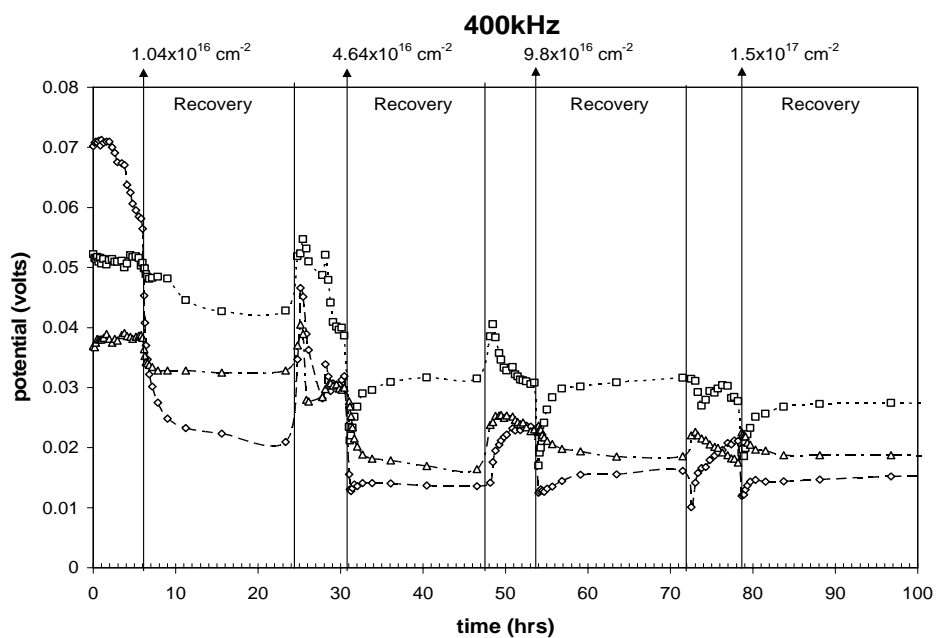


Figure 28. Irradiation response at 400 kHz

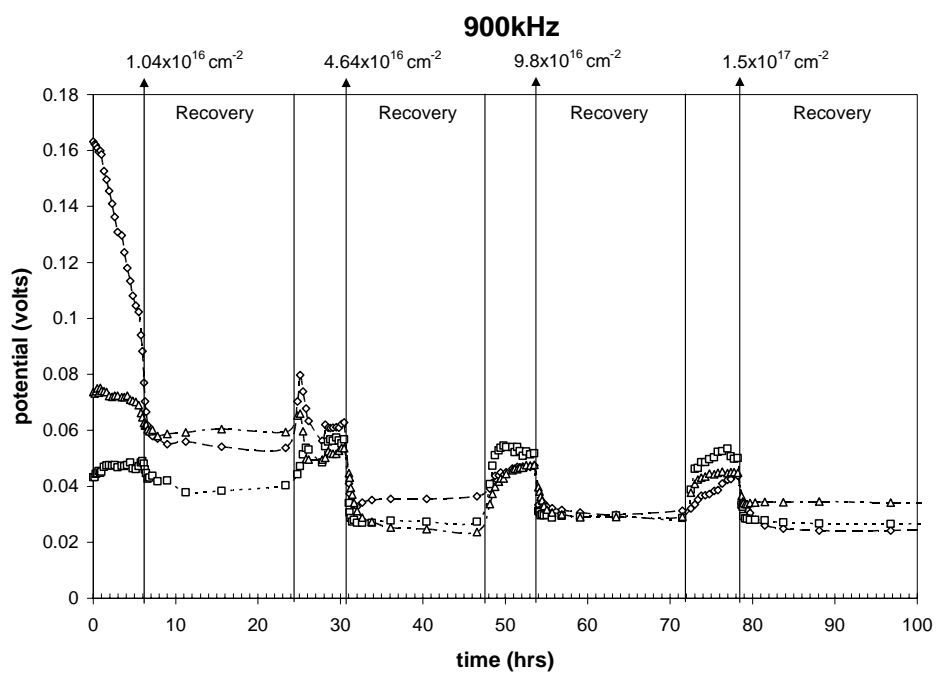


Figure 29. Irradiation response at 900 kHz

measured in volts, of the transducers to the acoustic pulse signal. Finally, the cumulative neutron fluence as a function of time is labeled at the end of each irradiation period and is summarized in table 7.

Table 7. Neutron fluence as a function of time

Time (hours)	Fluence (neutrons per cm ²)
6	1.04×10^{16}
31	4.64×10^{16}
53	9.8×10^{16}
78	1.5×10^{17}

A comparison of the initial response values at 400 kHz and 900 kHz with the in situ characterization in figure 30 shows very good correlation ensuring that nothing has happened to the waveguide apparatus and caused a change in coupling or performance since the characterization was performed.

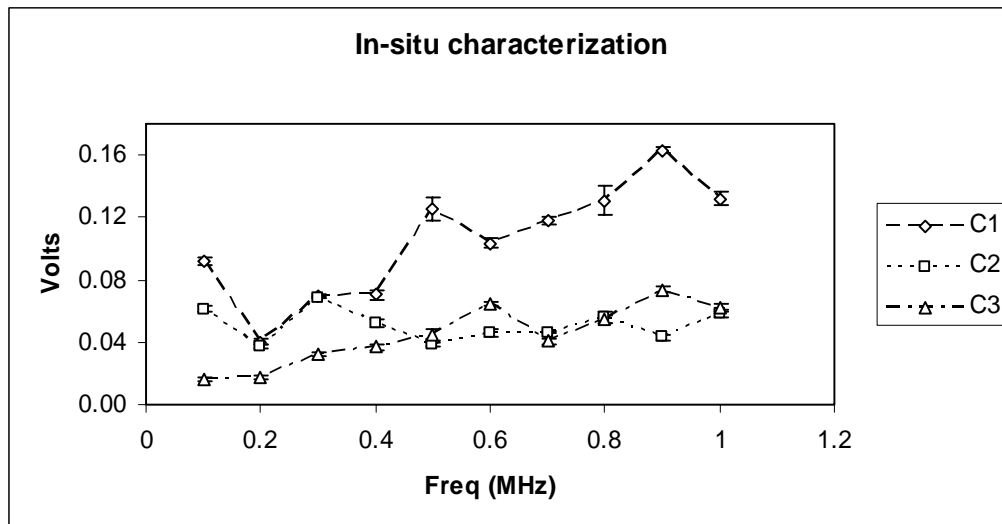


Figure 30. In situ characterization

It is apparent from the response measurements over time that transducers of the same design or series do not necessarily perform the same and are not affected by radiation quite the same. Although there are some distinct differences between each of the transducers at any given frequency, there are also some common trends.

Initial Phase Radiation Response.

During this phase, the response consistently degrades during irradiation. The rate of degradation varies between transducers and with frequency. When the reactor is shut down, recovery is poor which indicates that the damage to the transducer is permanent. Permanent damage is defined as failure to recover to the response level established prior to that session of irradiation.

A possible mechanism for the decrease in transducer response is illustrated in figure 36. The elimination of a ferroelectric dipole in the ceramic crystal lattice is

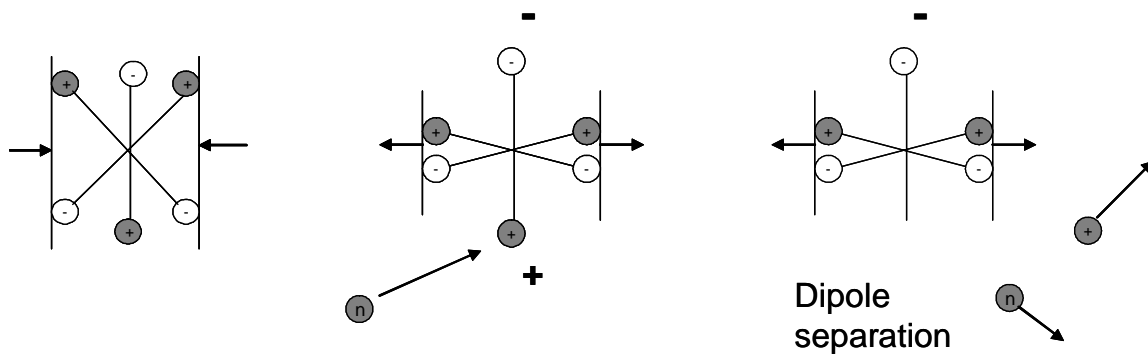


Figure 31. Neutron damage mechanism

accomplished by a neutron colliding with one of the dipole atoms and displacing it. The displaced atom is forced into the crystal lattice resulting in an interstitial and a vacancy.

As the dipole damage accumulates, the potential difference (voltage) generated in response to the acoustic pulse begins to deteriorate.

Intermediate Phase Radiation Response.

As degradation continues to occur at most frequencies, there is also an emerging pattern in the response. At some frequencies the response begins to increase as time of irradiation increases. It is interesting to note that regardless of whether the response is increasing or decreasing, when the reactor is shut down the response changes suddenly in the opposite direction of the trend. An example can be seen on channel 1 at 400 kHz. At the 50 hour and 75 hour time windows, channel 1 steadily increases in response until the reactor is shut down. The response immediately reduces by nearly 50% and then slowly shows some recovery. This observation suggests there is a transient effect occurring in the transducer which results in an artificial improvement in the transducers performance.

This phase is also marked by a sizable recovery but there is still indication of permanent damage. At 900 kHz, channel 1 and 2 both show a steadily increasing response trend in the 28 hour window. When the reactor is shut down, the response immediately decreases and then slowly begins to make a recovery but never reaches the same response level established prior to that session of irradiation.

Final Phase Radiation Response.

The transient effect that was observed in the intermediate phase is apparent during irradiation in almost every frequency. When the reactor is shut down the response returns to nearly the same level it was prior to that session of irradiation. This can be observed in the 60 and 90 hour windows at both 400 kHz and 900 kHz. Since the

transducers recover to the response level established prior to that session of irradiation, no further permanent damage is being inflicted on them.

A possible mechanism for the transient effect on response that is observed is depicted in figure 32. The displacement damage created by neutron radiation becomes a trap for the charge carriers produced by ionizing radiation. The trapped charge temporarily replaces the atom that was dislocated from the ferroelectric crystal cell and restores the dipole moment. As irradiation time increases, displacement damage

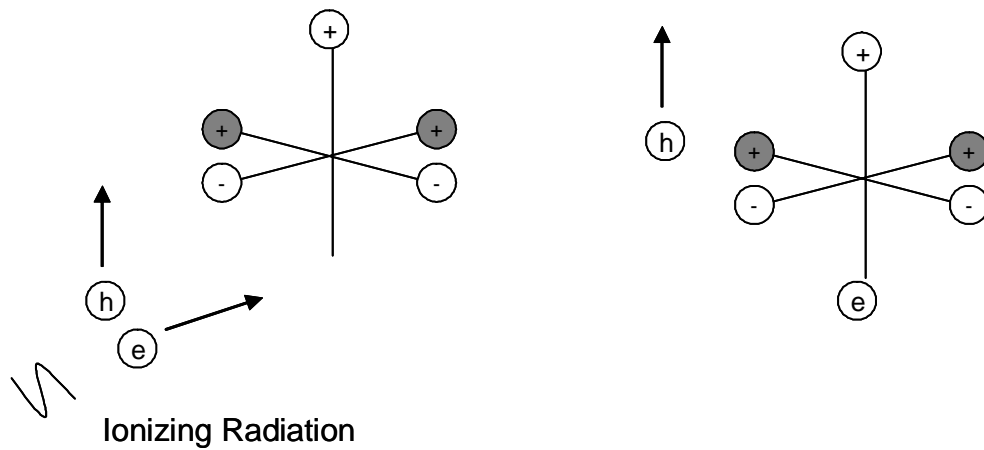


Figure 32. Transient effect caused by ionizing radiation

increases resulting in more trapped charge intermediates and an increasing piezoelectric response. When the reactor is shut down, the rate of ionization decreases and recombination of charge carriers eliminates the temporary dipoles resulting in an immediate decrease in transducer response.

Although all three transducers exhibited these general trends, they did not necessarily arrive at each phase at the same time. This is also the case for each

transducer with regard to frequency. Some frequencies reached permanent damage equilibrium prior to others and some frequencies never reached damage equilibrium at all, as was the case with C2 at 300 kHz (Appendix A).

Appendix B compares the relative response change of the transducers at various dose rates for each frequency. Since each transducer has a unique response for each frequency, plotting the relative response change will allow better comparison of irradiation effects between the three transducers. If there are any trends in response change which show a frequency or dose rate dependence, it should become apparent in the data that has been graphed.

Unfortunately, no frequency dependant trends were consistently identified for all three transducers. The graphs do offer a better understanding of how all frequencies are being affected for each transducer however. At the end of irradiation, channel 1 clearly indicates that the transient increased response is frequency dependant for that transducer. Low frequencies do not experience increased response while higher frequencies are increased substantially (figures 65 and 68). This is not true for the other two transducers however.

V. Conclusions and Recommendations

Conclusions

Permanent damage to the transducers resulted from exposure to the radiation field inside the OSURR as noted by the degradation of response at all frequencies tested on each transducer. Based on the assumption that gamma radiation effects are transient, the damage must be neutron induced and is therefore probably caused by displacement of atoms in the lead metaniobate crystal lattice.

At the beginning of irradiation it was suspected that the pyroelectric effect, caused by joule heating during irradiation, may be responsible for some of the degradation in transducer response. To determine if this was likely or not, dose rate was calculated (J/kg) and then divided by the specific heat of lead metaniobate (J/kg C). The rate of temperature increase at full reactor power was determined to be one degree every 482 seconds (Appendix E).

A heat transfer calculation was done on the system at full power to see how high the surface temperature of the waveguide/transducer apparatus would rise before reaching equilibrium with the surrounding air. The air temperature was assumed to be the same as the cooling pool. An aluminum tubing wall separates the air from the pool and the pool is considered to be an infinite heat sink. The results show that the expected temperature increase from joule heating is not more than 1 degree K.

During the first day of irradiation the power was at 50 kW for three hours and 100 kW for another three hours. This was the period in which most response degradation occurred. The rate of calculated temperature increase would have been 72 minutes and 36

minutes per degree K respectively. These calculations do not support the possibility of the pyroelectric effect causing response degradation. Furthermore, the thermal effects experiment conducted after irradiation showed that the transducer had the same response profile at 100°C as at room temperature when couplant was used indicating the pyroelectric effect is negligible and transducer internal expansion is not responsible for changes in response during thermal heating. Coupling changes due to thermal heating did change the response of the transducers, but probably had no impact during the irradiation experiment because the calculated rate of heat transfer exceeded the rate at which heat was being generated in the transducers.

The transducers received a total neutron dose of 392 krad after four days of irradiation (see Appendix D for calculations). Although response was significantly reduced, the devices never reached a point where they failed to give a reproducible response with a standard deviation that was less than 10% of the mean value measured. The oscilloscope's minimum voltage resolution is 2 mV while the lowest response recorded during the experiment was about 10 mV. If the response had continued to degrade, there was still 40 dB of signal amplification available in the signal processing equipment that was never used. The signal-to-noise ratio was also very good as indicated by the small standard deviations during sampling. The transducer's dose limit is therefore greater than 392 krad.

Recovery from displacement damage was not complete for any of the transducers although channel 1 (sn10) seemed to receive much more damage than the other two. But it was also significantly more sensitive than the others at the beginning of the experiment.

With additional time, the transducers may recover a little more but it is unlikely they will ever regain their original sensitivity. It may be possible to produce more annealing with a higher temperature but room temperature is not adequate.

System coupling caused the most difficulty of any other effect during the execution of this experiment. Coupling changes during thermal characterization created much confusion about what was causing transducer response degradation. It caused the false conclusion that the transducers were permanently damaged from joule heating. It also led to investigating the pyroelectric effect as a possible cause of degraded response.

The idea of using an aluminum rod as a waveguide for in situ neutron damage testing was remarkably successful. The system was reliable and provided consistent and very reproducible results. It was rugged, simple, reusable, and easy to construct.

The data sampling method was also very successful in producing measurements with a small standard deviation. Unfortunately, it required many hours of manual data processing and consumed a large amount of time in preparation.

Recommendations

Although the primary effect of neutron radiation is displacement damage, it also causes ionization. Likewise, ionizing radiation also causes some displacement. Because of this, it is difficult to distinguish which type of radiation is responsible for the various effects that were observed in the results of the experiment.

An in situ gamma radiation characterization on the transducers before reactor irradiation would help to delineate gamma induced effects from neutron effects. In this way it would be possible to observe how gamma radiation affects transducer response

prior to displacement damage. This information would help considerably in understanding the impact that neutrons have on the performance of the transducers.

Furthermore, another in situ gamma radiation characterization after irradiation in the reactor would offer even more information on neutron damage because it could be compared to the characterization when there was no neutron damage. Any difference would be directly attributable to neutron displacement damage.

An extended in situ gamma radiation study might also provide information on whether ionizing radiation is causing conductivity changes in insulating materials inside the transducer. Reduced response magnitudes would not necessarily show that leakage current is increasing because of the possibility of other damage mechanisms, but if response magnitudes did not decrease it would show that leakage current is not a damage mechanism.

A thermocouple could be added in the neutron port so that thermal effects could be measured directly instead of being deduced. Although it is not possible to measure the piezoelectric element directly because it is encased in the transducer, a thermocouple wire attached to the aluminum bar in close proximity to the transducers would give a very close approximation since the metal case of the transducer will rapidly conduct any significant heat to the waveguide.

An investigation into the effects of radiation on potential radiation resistant couplants could also prove to be very beneficial. If coupling changes are occurring due to thermal expansion during irradiation, then applying a couplant would eliminate the

problem and provide more accurate results. But first it needs to be shown that the couplant properties do not change with irradiation.

Processing the raw sampling data was very time intensive and prone to error because it was not automated. A great amount of time was also spent in developing the sampling system and making it work. Much more experimentation could have been accomplished if an acoustic emission measuring system were simply purchased. This would allow more time to be spent for conducting in situ gamma cell irradiations or multiple neutron damage assessments.

Finally, having data on charge carrier generation rate and mobility in lead metaniobate would be very helpful in investigating damage mechanisms that involve bulk trapped charge and charge migration. Follow on research for this project could include developing an experiment to gather this kind of information and could contribute to a better understanding of the neutron damage mechanism to lead metaniobate.

Appendix A: Irradiation Data

The log of irradiation of the transducers is shown in table 8. The changes in the power of the reactor are sequential; meaning that irradiation always started at a lower power and progressed to the highest power. Initially, the plan required the power to be kept at 50 kW until a fluence of 10^{15} was achieved, which is the equivalent neutron fluence in a single pulse at the ACRR. Afterwards, the power would be increased to maximum (450 kW) to achieve as much fluence as possible in the scheduled time (4 days) for irradiation. The plan had to be altered because of high radiation levels occurring outside the reactor due to streaming radiation from the neutron port.

On day two, shielding was increased around the neutron port which reduced the radiation levels to an acceptable level and allowed the power to eventually be increased to maximum.

Table 8. Irradiation schedule

Day	Power (kW)	Time (sec)	Flux	Fluence	Total Fluence
1	50	11,220	2.68E11	3.011E15	
	100	7800	5.37E11	4.186E15	
	200	3000	1.07E12	3.2E15	1.04E16
2	100	600	5.37E11	3.2E14	
	200	2400	1.07E12	2.58E15	
	300	3600	1.61E12	5.8E15	
	400	1200	2.147E12	2.58E15	
	450	10,200	2.415E12	2.46E16	4.64E16
3	450	21,600	2.415E12	5.2E16	9.82E16
4	450	21,600	2.415E12	5.2E16	1.5E17

The irradiation data is shown plotted by frequency in figures 33 through 40.

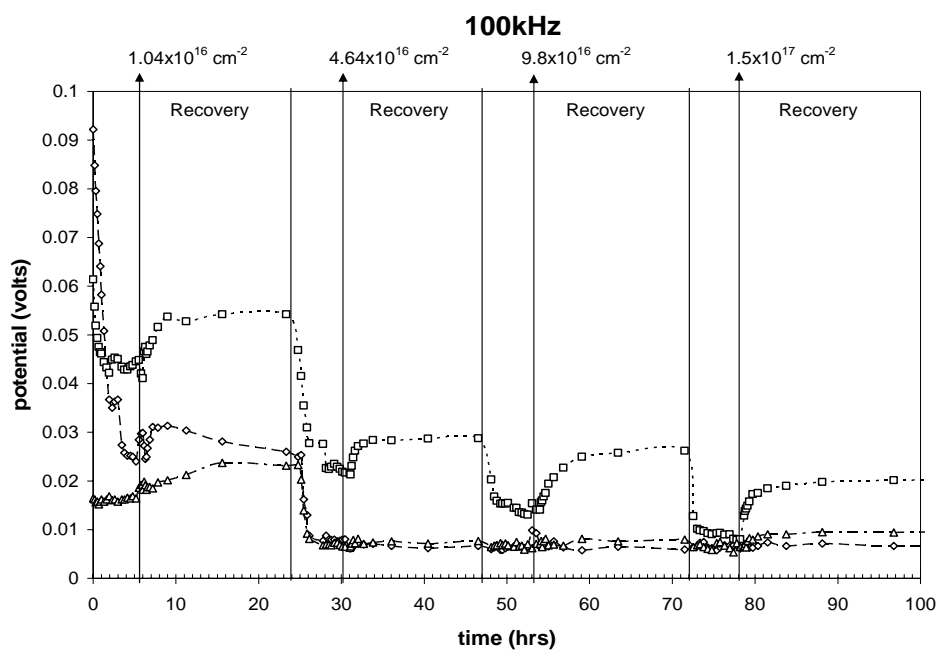


Figure 33. Irradiation response at 100 kHz

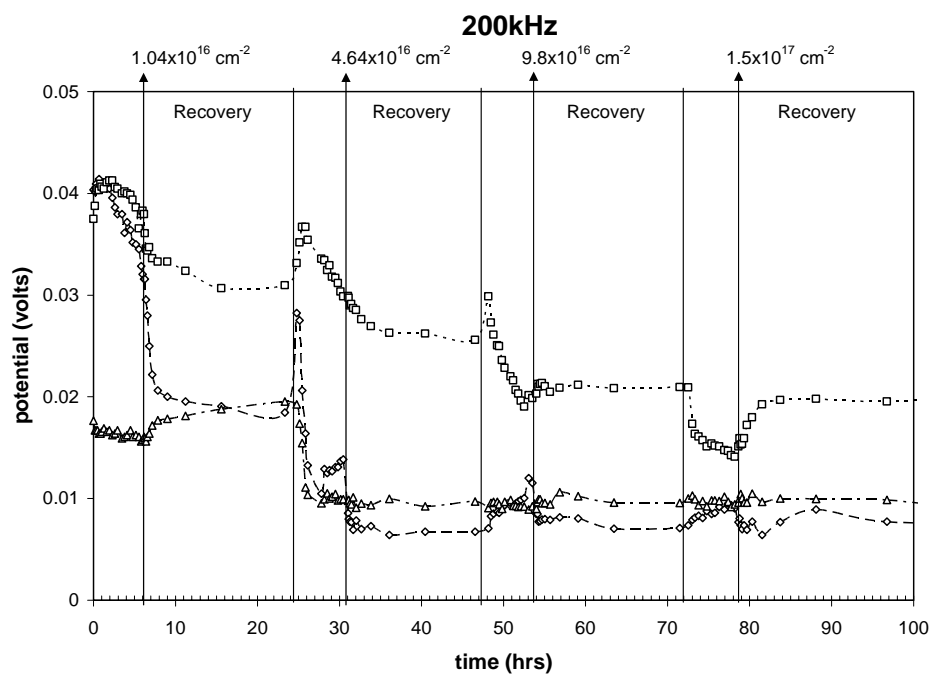


Figure 34. Irradiation response at 200 kHz

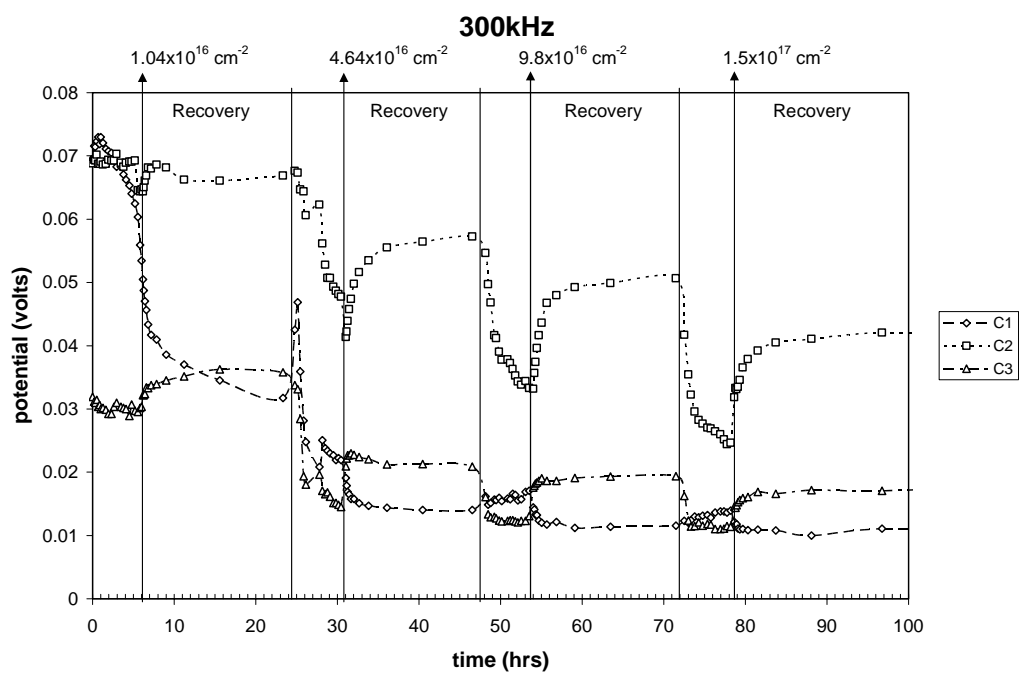


Figure 35. Irradiation response at 300 kHz

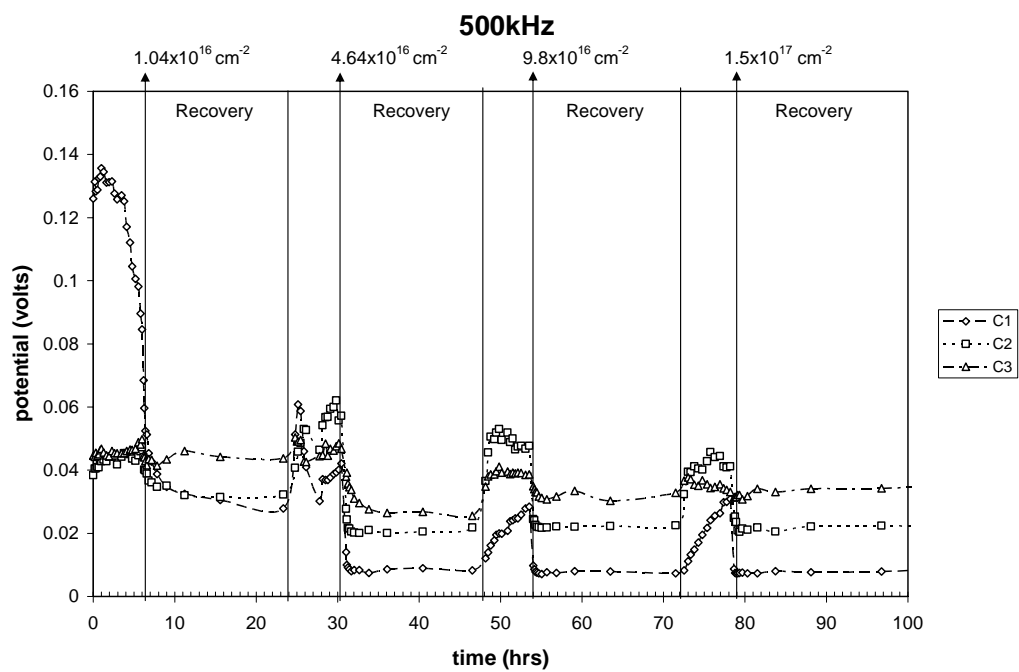


Figure 36. Irradiation response at 500 kHz

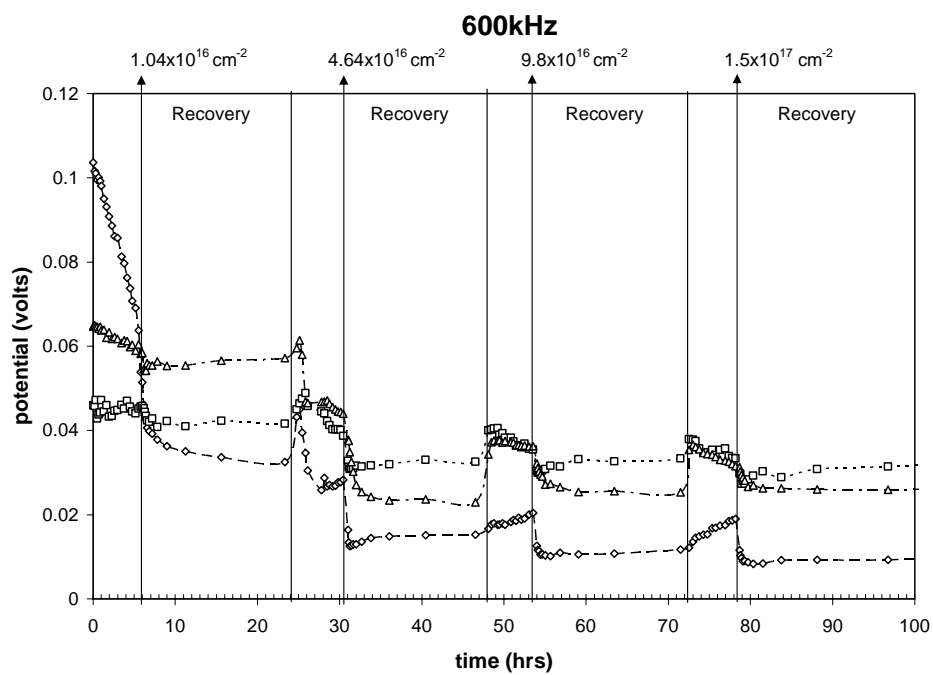


Figure 37. Irradiation response at 600 kHz

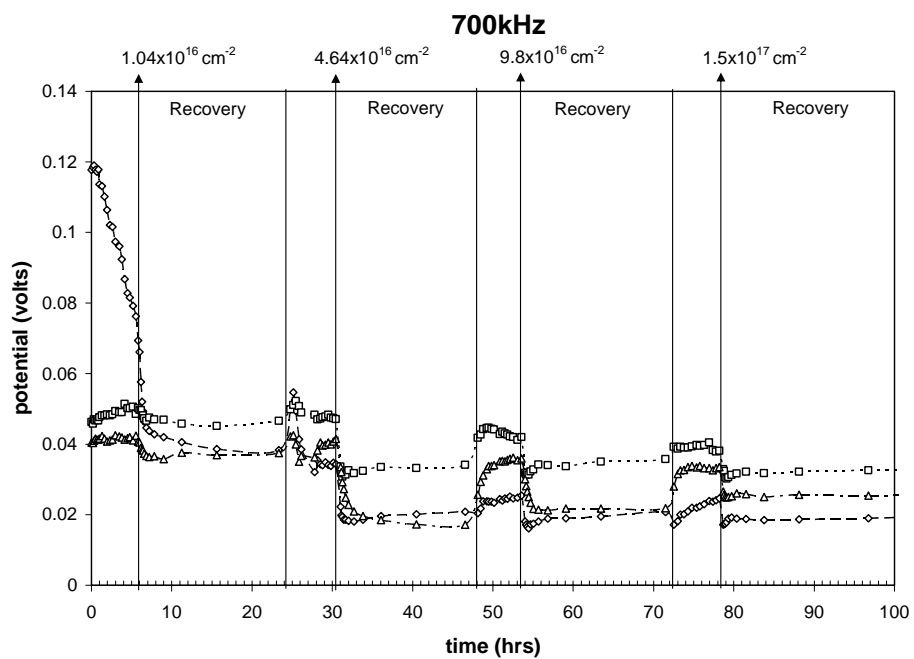


Figure 38. Irradiation response at 700 kHz

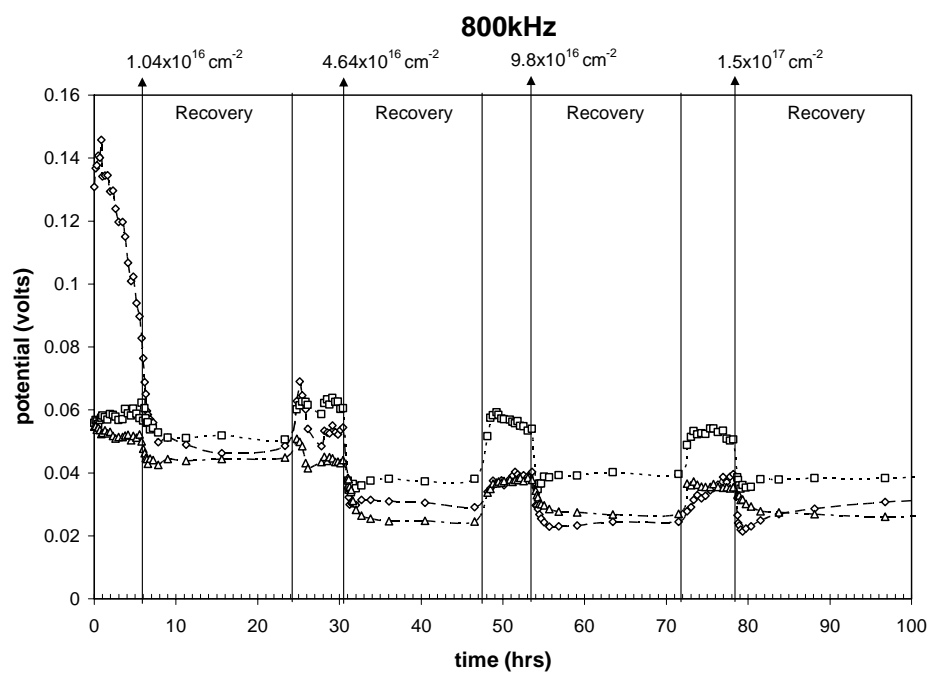


Figure 39. Irradiation response at 800 kHz

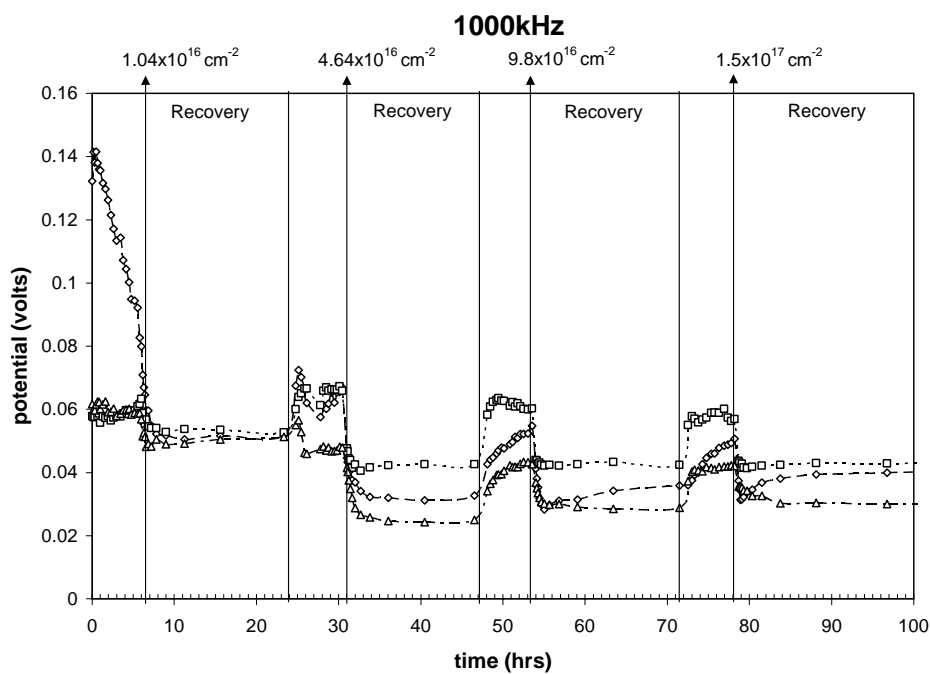


Figure 40. Irradiation response at 1 MHz

Appendix B: Relative Response Change by Frequency

The relative response change at various dose rates is compared in two frequency groups for each of the three channels used. Figures 41 through 70 summarize the response change of the three transducers during the four days of irradiation. The data is plotted in two frequency groups to reduce the amount of data given in one graph and to help in identifying trends that may be related to low or high frequencies. The lower frequency group consists of 100 thru 500 kHz and the higher frequency group is 600 thru 1000 kHz.

The initial response voltage (V_o) used in plotting the data is taken from the first data sampling for that day of irradiation. It is important to remember that on day 1 and day 2 the dose rate was being progressively increased, so V_o represents the initial response at the initial dose rate. Table 8 in appendix A shows the progression of irradiation. The power levels that are plotted were selected because enough data was taken to show any possible trends. For instance, on day 2 the power was not kept at 100, 200, 300, or 400 kilowatts long enough to collect sufficient data for plotting.

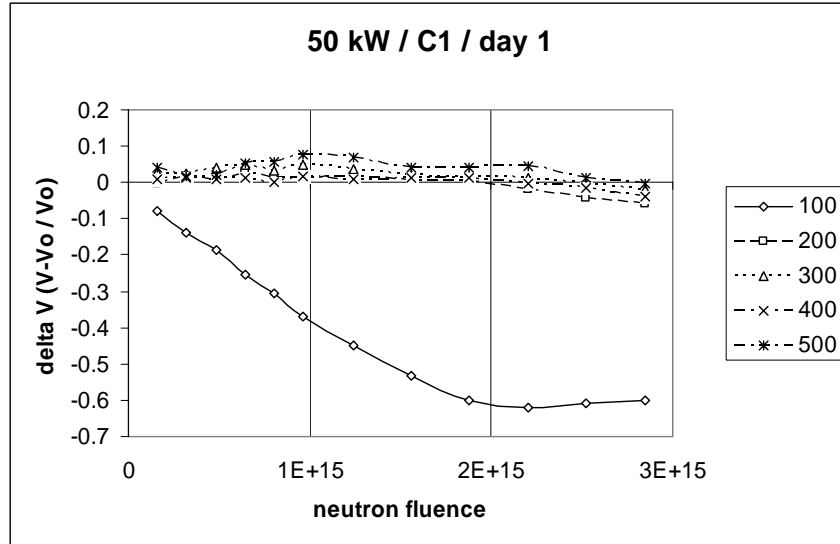


Figure 41. C1 lower frequency response change at 50 kW

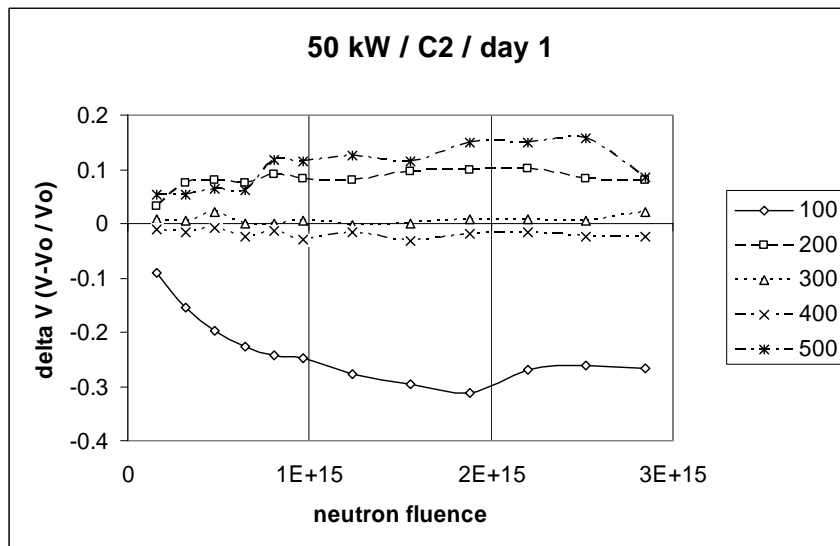


Figure 42. C2 lower frequency response change at 50 kW

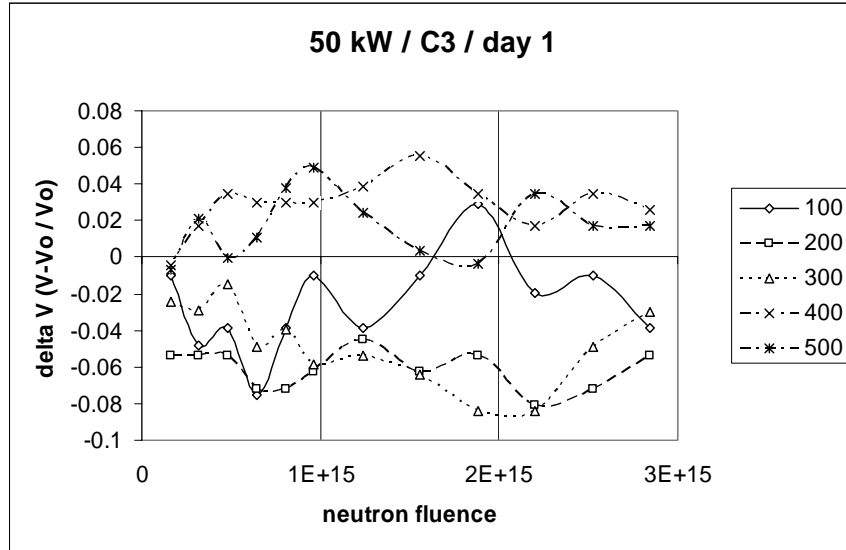


Figure 43. C3 lower frequency response change at 50 kW

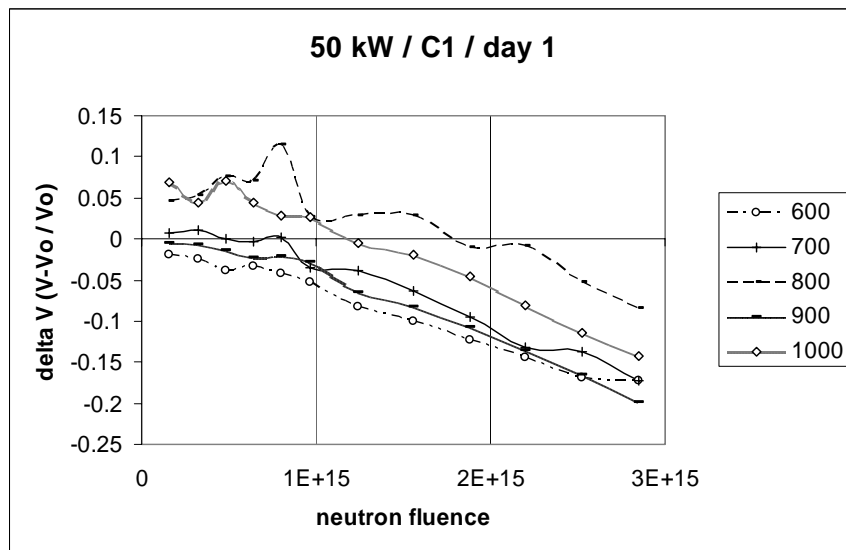


Figure 44. C1 higher frequency response change at 50 kW

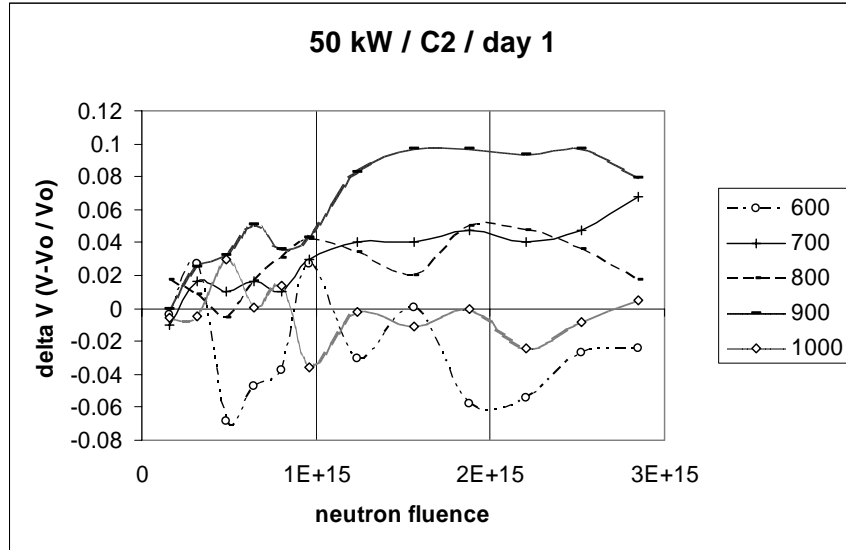


Figure 45. C2 higher frequency response change at 50 kW

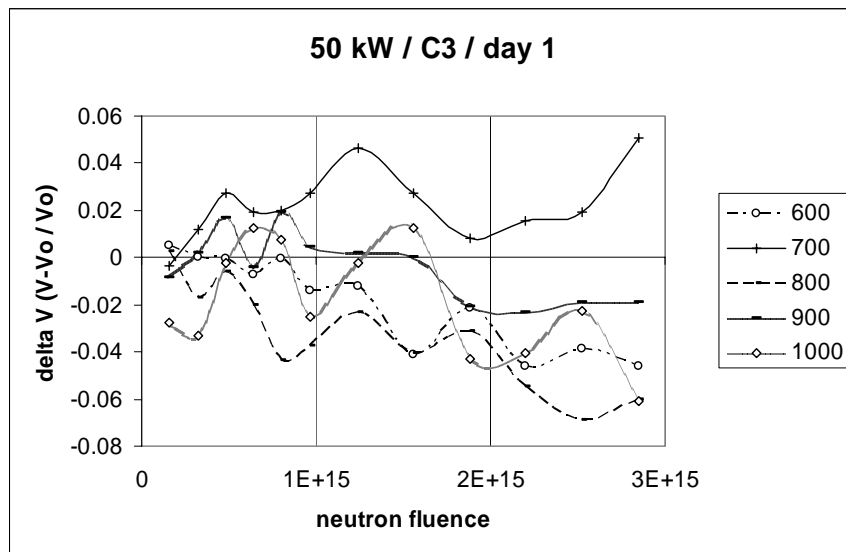


Figure 46. C3 higher frequency response change at 50 kW

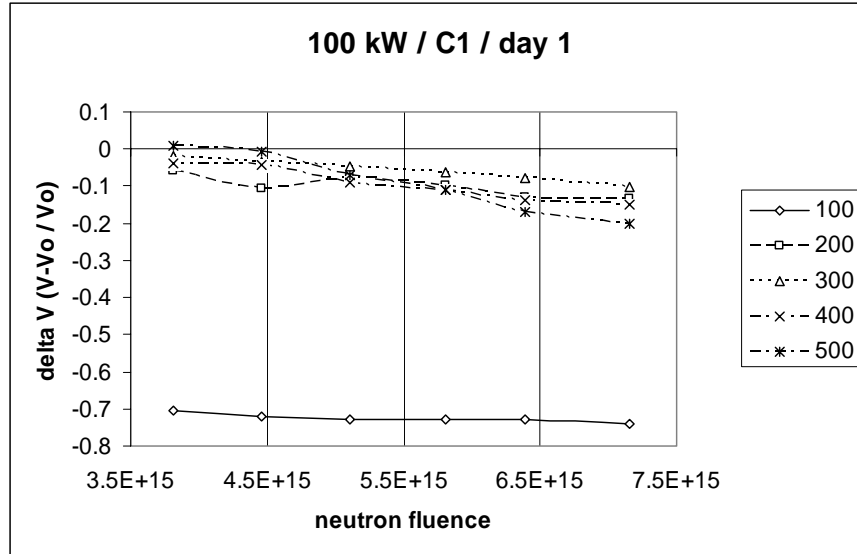


Figure 47. C1 lower frequency response change at 100 kW

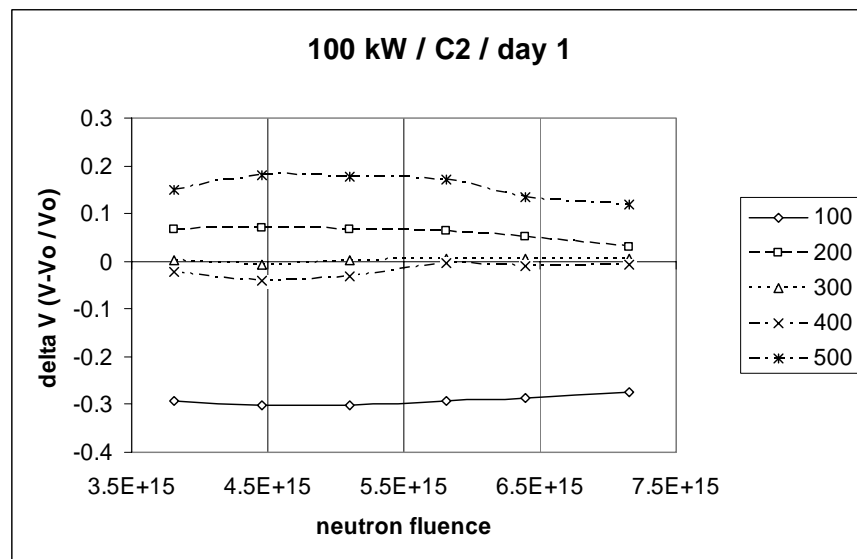


Figure 48. C2 lower frequency response change at 100 kW

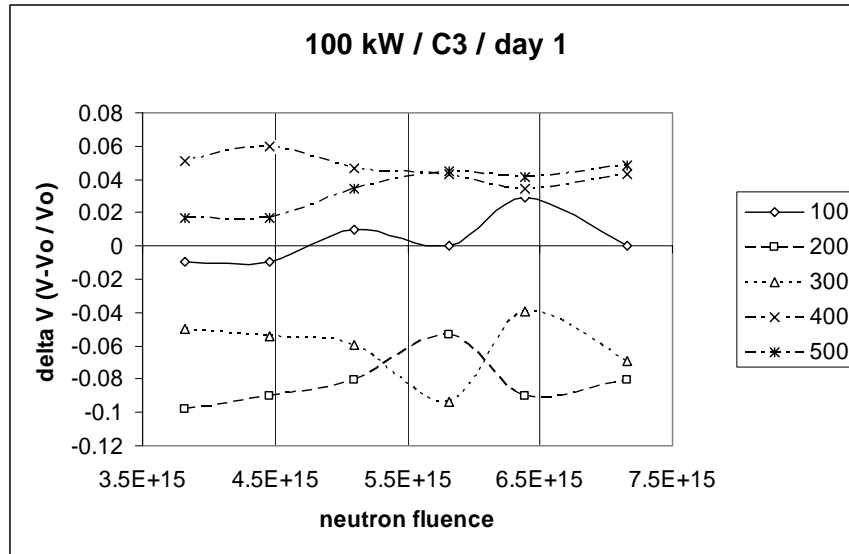


Figure 49. C3 lower frequency response change at 100 kW

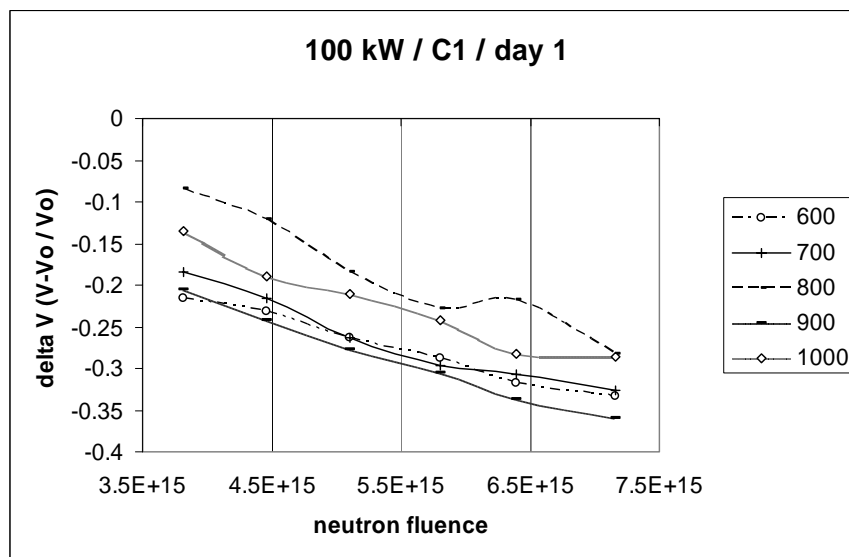


Figure 50. C1 higher frequency response change at 100 kW

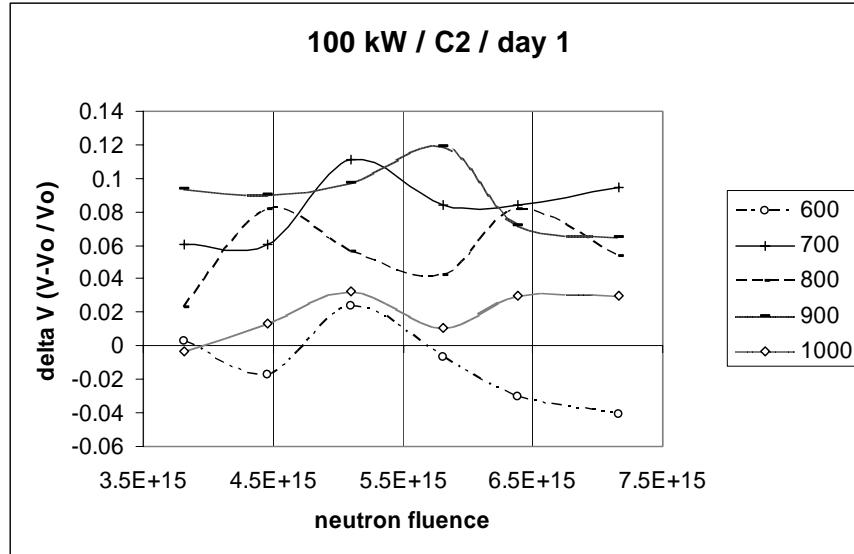


Figure 51. C2 higher frequency response change at 100 kW

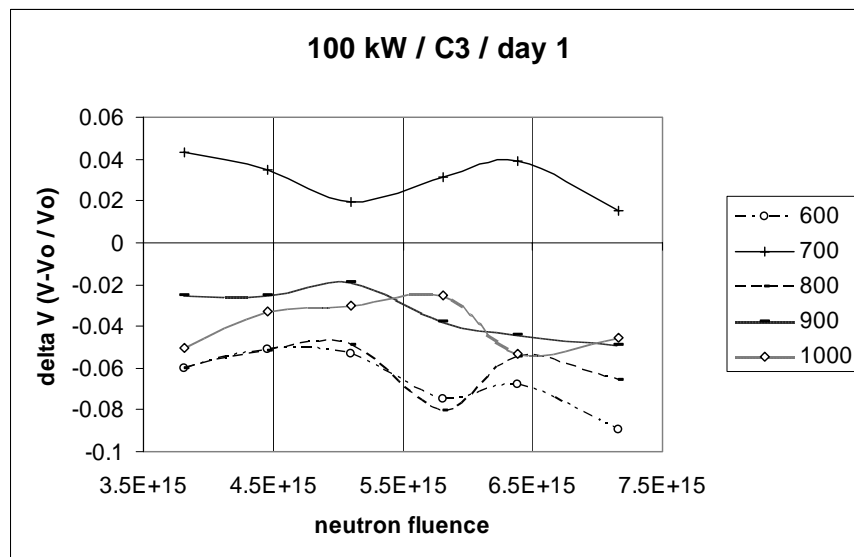


Figure 52. C3 higher frequency response change at 100 kW

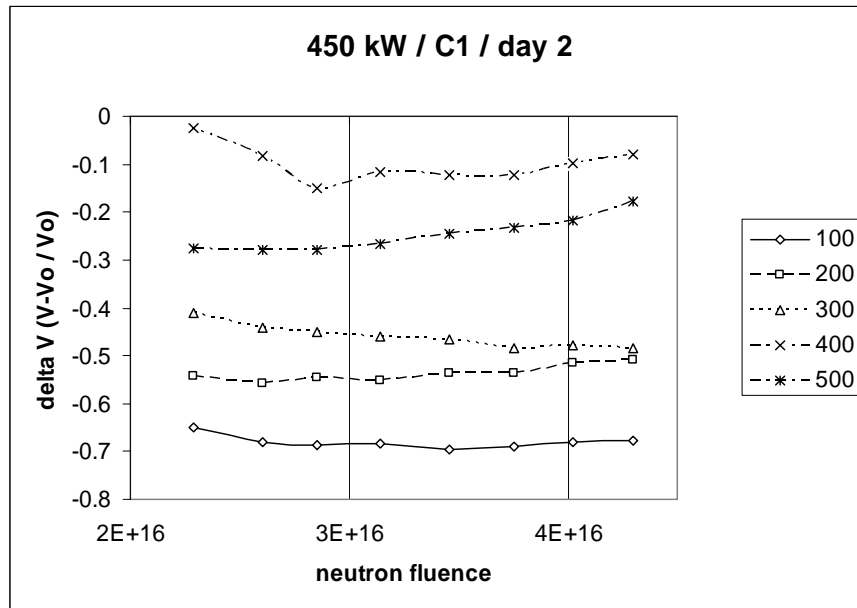


Figure 53. C1 lower frequency response change at 450 kW on day 2

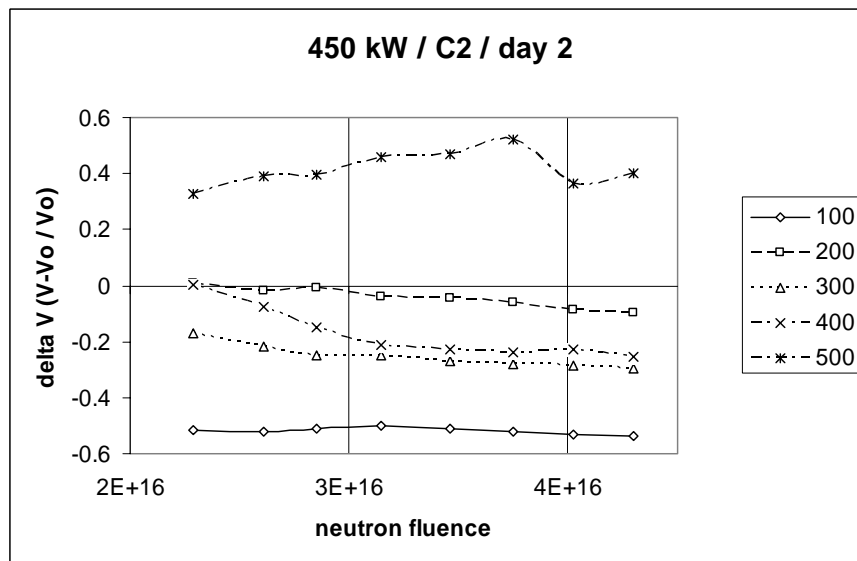


Figure 54. C2 lower frequency response change at 450 kW on day 2

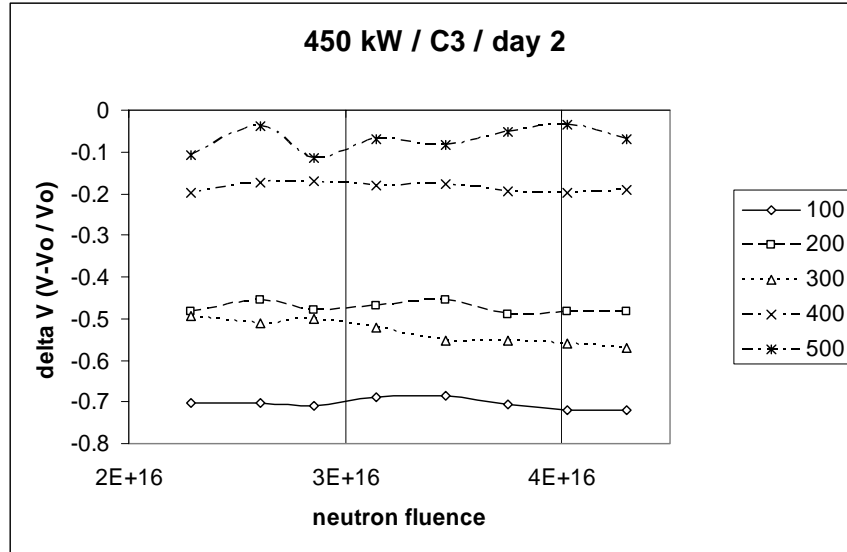


Figure 55. C3 lower frequency response change at 450 kW on day 2

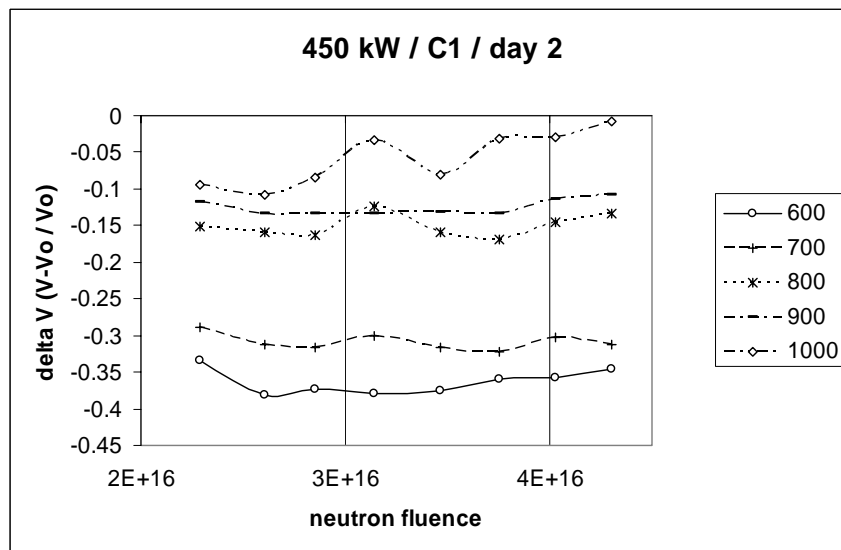


Figure 56. C1 higher frequency response change at 450 kW on day 2

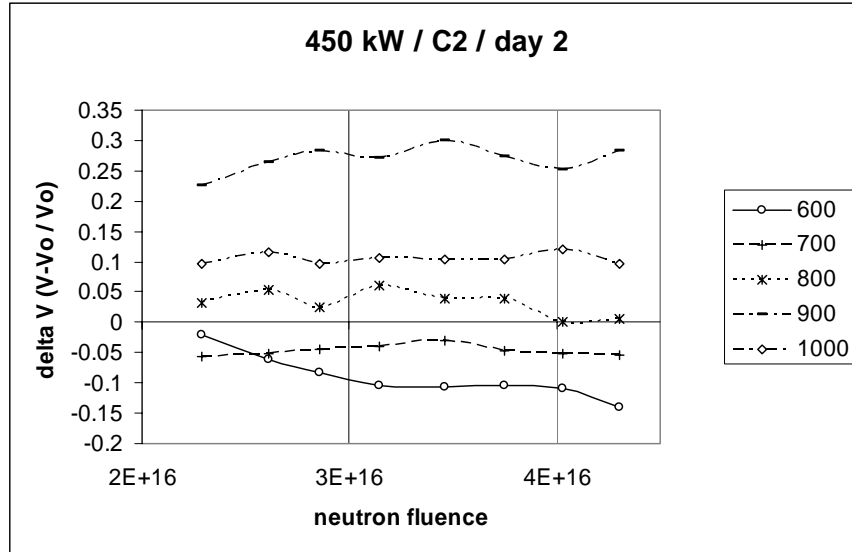


Figure 57. C2 higher frequency response change at 450 kW on day 2

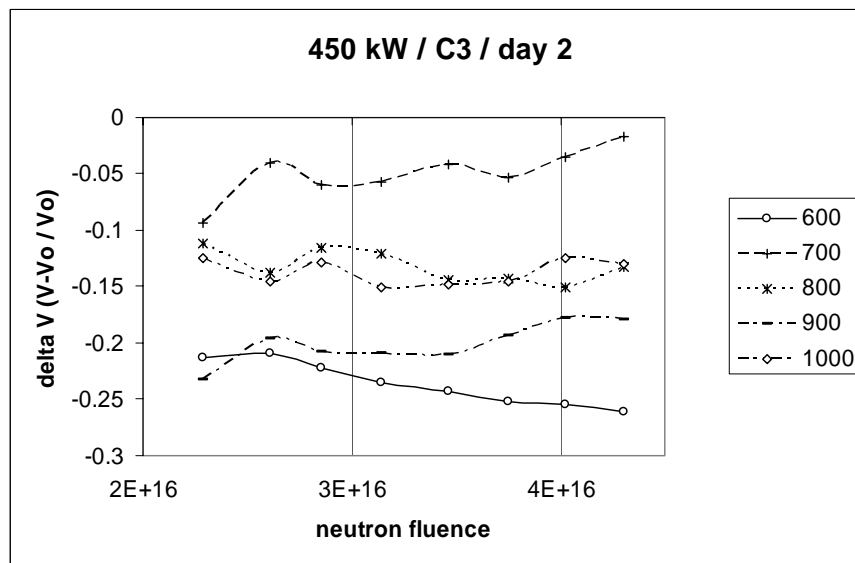


Figure 58. C3 higher frequency response change at 450 kW on day 2

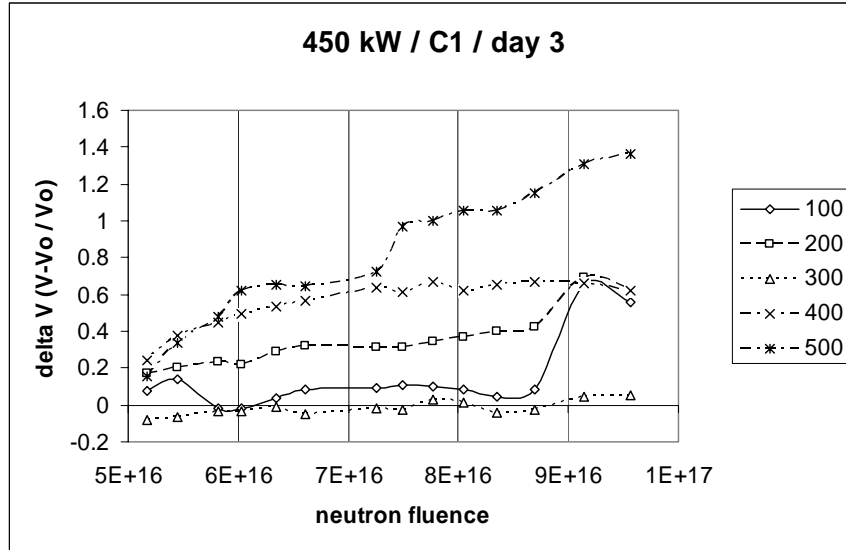


Figure 59. C1 lower frequency response change at 450 kW on day 3

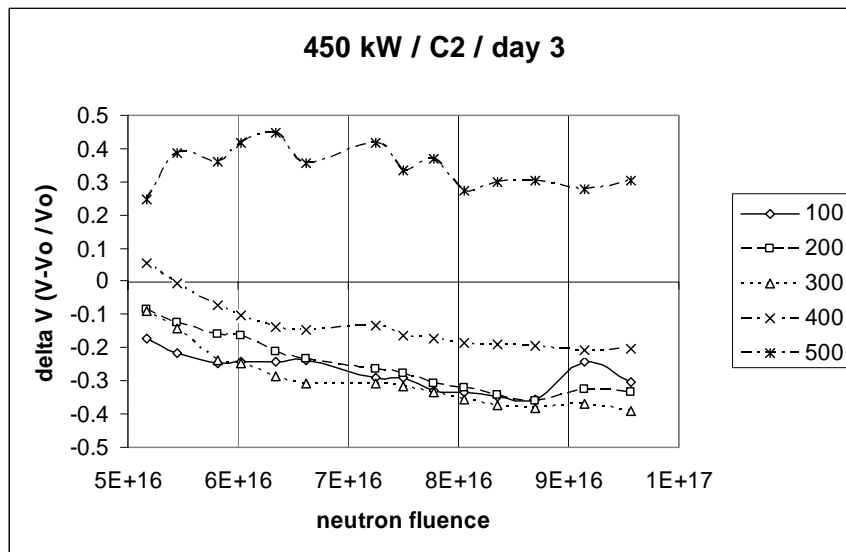


Figure 60. C2 lower frequency response change at 450 kW on day 3

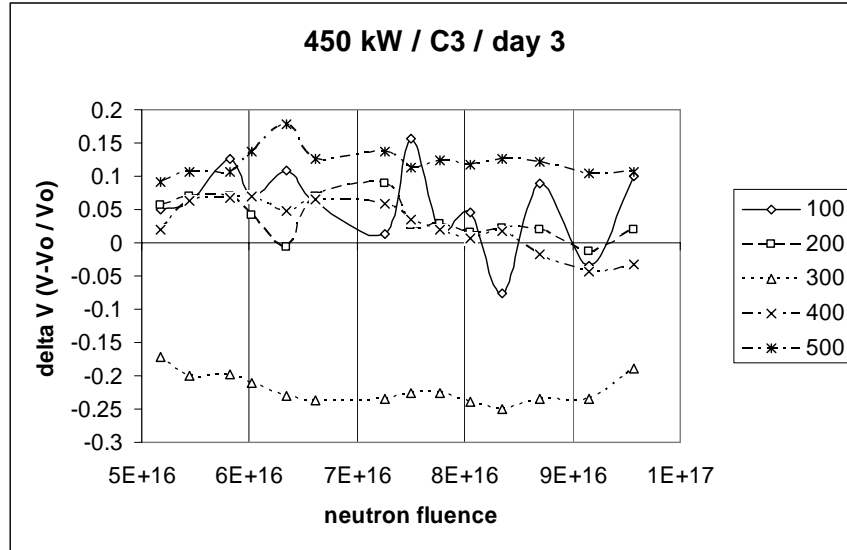


Figure 61. C3 lower frequency response change at 450 kW on day 3

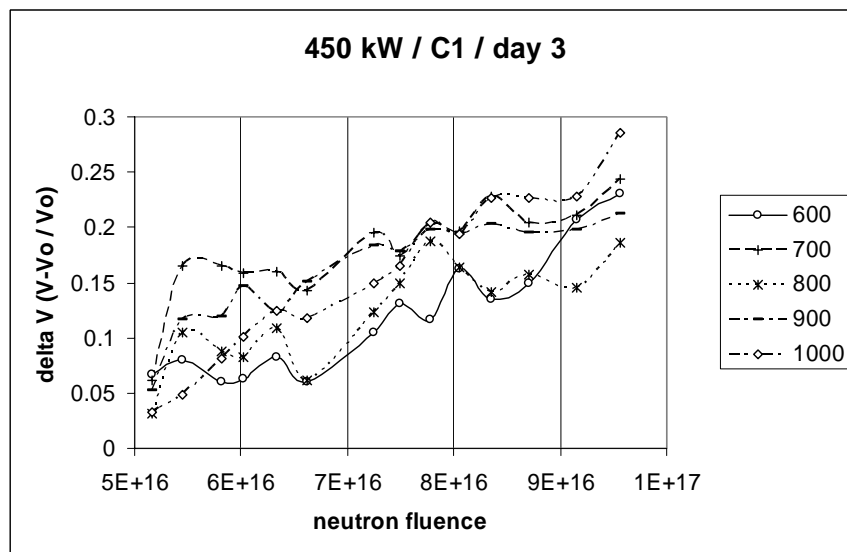


Figure 62. C1 higher frequency response change at 450 kW on day 3

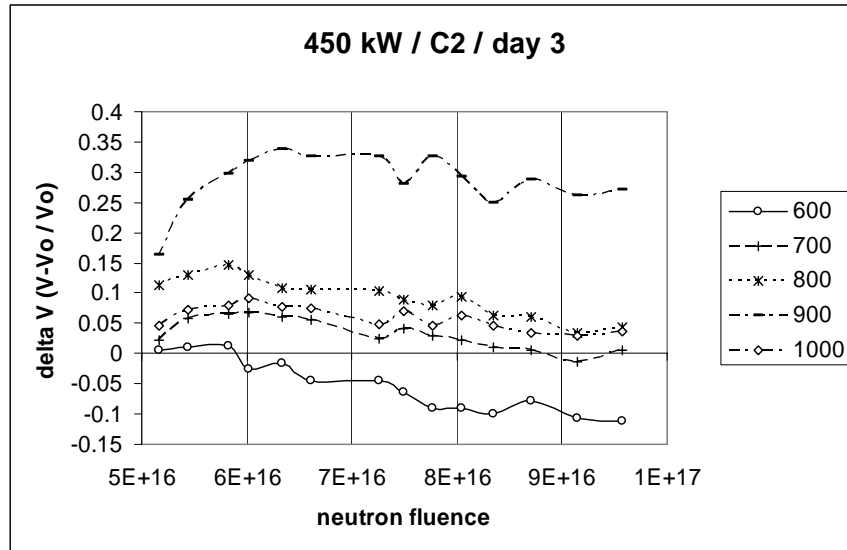


Figure 63. C2 higher frequency response change at 450 kW on day 3

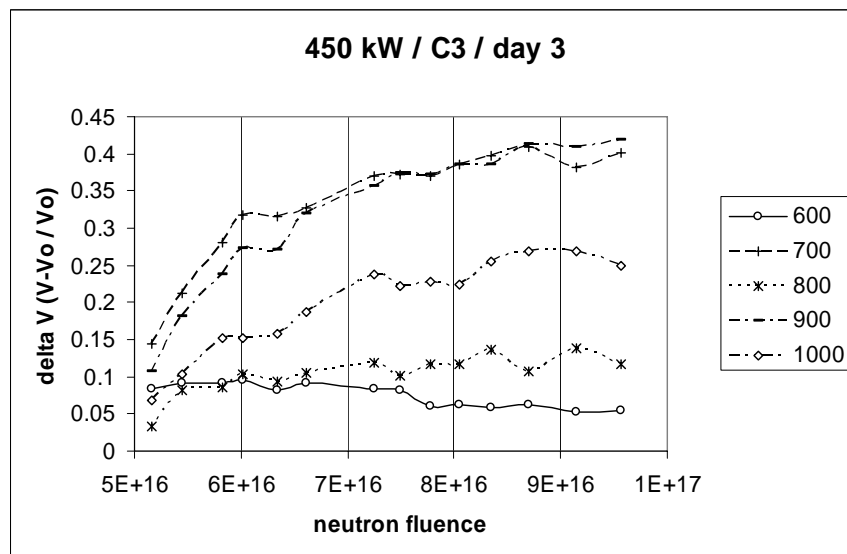


Figure 64. C3 higher frequency response change at 450 kW on day 3

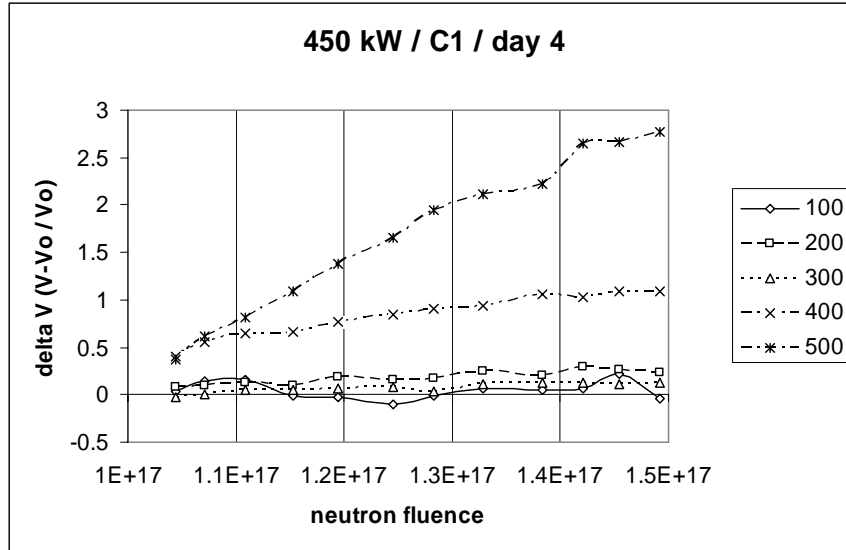


Figure 65. C1 lower frequency response change at 450 kW on day 4

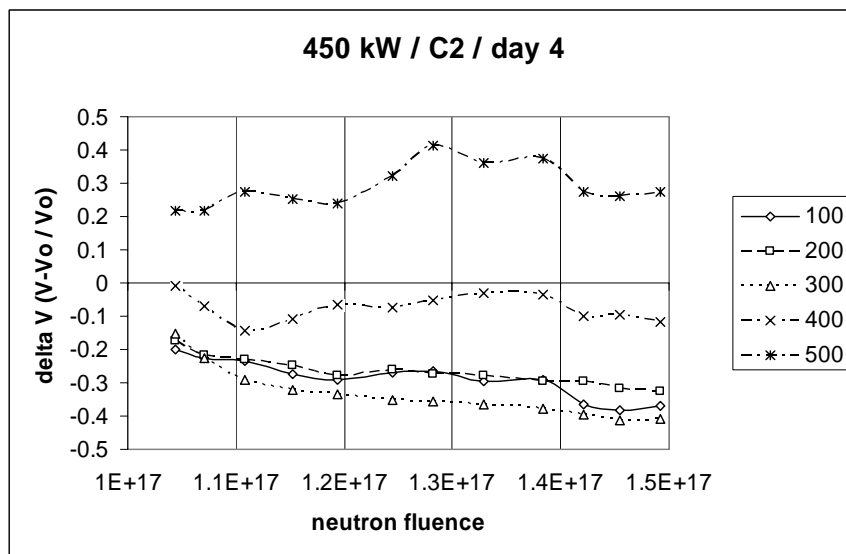


Figure 66. C2 lower frequency response change at 450 kW on day 4

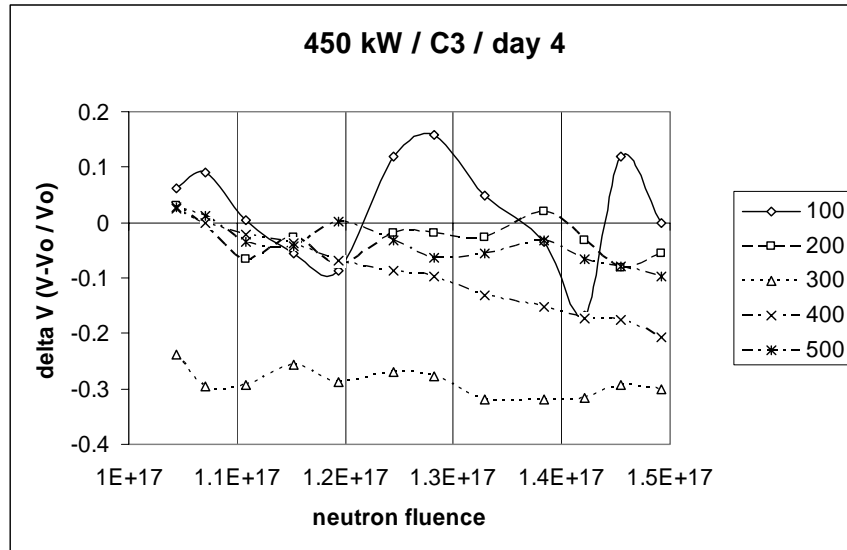


Figure 67. C3 lower frequency response change at 450 kW on day 4

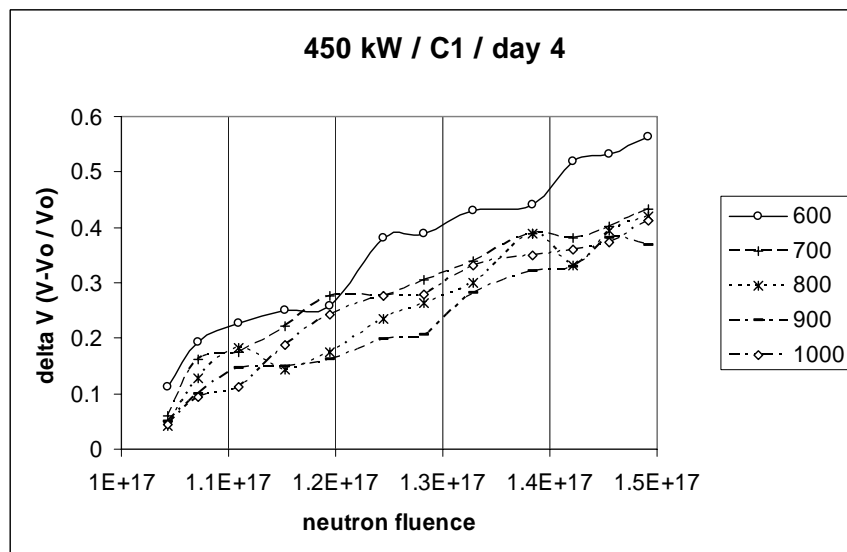


Figure 68. C1 higher frequency response change at 450 kW on day 4

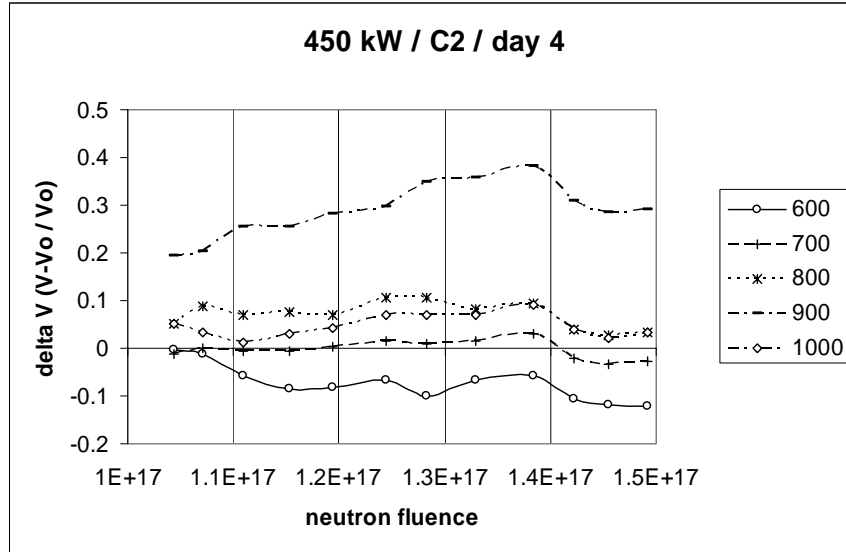


Figure 69. C2 higher frequency response change at 450 kW on day 4

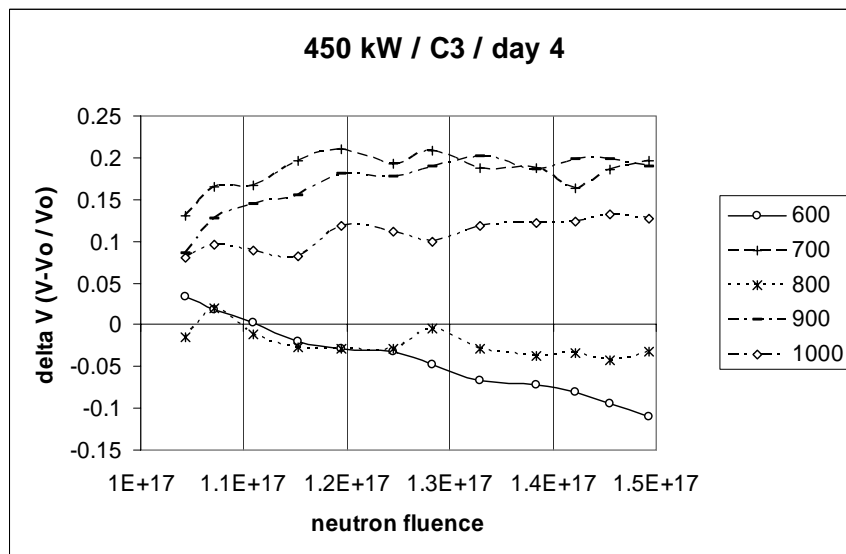


Figure 70. C3 higher frequency response change at 450 kW on day 4

Appendix C: Macroscopic Cross Section for Lead Metaniobate

PbNb₂O₆ properties:

$$\rho := 6.2 \cdot \frac{\text{gm}}{\text{cm}^3}$$

$$\text{GAW} := 207 \cdot \frac{\text{gm}}{\text{mol}} + (2 \cdot 93) \cdot \frac{\text{gm}}{\text{mol}} + (6 \cdot 16) \cdot \frac{\text{gm}}{\text{mol}}$$

$$\text{GAW} = 489 \frac{\text{gm}}{\text{mol}}$$

Element weight fractions:

$$\text{Pb: } \frac{207 \cdot \text{gm}}{489 \cdot \text{gm}} = 0.423 \quad \text{Nb: } \frac{186 \cdot \text{gm}}{489 \cdot \text{gm}} = 0.38 \quad \text{O: } \frac{96 \cdot \text{gm}}{489 \cdot \text{gm}} = 0.196$$

Element densities per unit volume

PbNb₂O₆ :

$$\rho_{\text{Pb}} := \rho \cdot \frac{207 \cdot \text{gm}}{489 \cdot \text{gm}} \quad \rho_{\text{Nb}} := \rho \cdot \frac{186 \cdot \text{gm}}{489 \cdot \text{gm}} \quad \rho_{\text{O}} := \rho \cdot \frac{96 \cdot \text{gm}}{489 \cdot \text{gm}}$$

$$\rho_{\text{Pb}} = 2.625 \frac{\text{gm}}{\text{cm}^3} \quad \rho_{\text{Nb}} = 2.358 \frac{\text{gm}}{\text{cm}^3} \quad \rho_{\text{O}} = 1.217 \frac{\text{gm}}{\text{cm}^3}$$

The macroscopic cross section for an individual element in determining the atom density and multiplying by

PbNb₂O₆ is found by the microscopic cross section :

$$N_{\text{Nb}} := 6.022 \cdot 10^{23} \cdot \text{mol}^{-1} \cdot \rho_{\text{Nb}} \cdot \frac{1}{\text{GAW}} \quad \text{Niobium atom density.}$$

$$\sigma_{\text{Nb20MeV}} := 3.48 \cdot 10^{-24} \cdot \text{cm}^2 \quad \text{microscopic cross section for Nb at 20 MeV.}$$

$$\Sigma_{\text{Nb}} := N_{\text{Nb}} \cdot \sigma_{\text{Nb20MeV}}$$

$$\Sigma_{\text{Nb}} = 0.01 \text{ cm}^{-1}$$

So, calculate the atom density of each element to use in determining the macroscopic cross section for that element in lead metaniobate:

$$N_{\text{Pb}} := 6.022 \cdot 10^{23} \cdot \text{mol}^{-1} \cdot \rho_{\text{Pb}} \cdot \frac{1}{\text{GAW}}$$

$$N_{\text{Pb}} = 3.232 \times 10^{21} \text{ cm}^{-3} \quad (\text{more to follow on Pb})$$

$$N_{\text{Nb}} := 6.022 \cdot 10^{23} \cdot \text{mol}^{-1} \cdot \rho_{\text{Nb}} \cdot \frac{1}{\text{GAW}}$$

$$N_{\text{Nb}} = 2.904 \times 10^{21} \text{ cm}^{-3}$$

$$N_{\text{O}} := 6.022 \cdot 10^{23} \cdot \text{mol}^{-1} \cdot \rho_{\text{O}} \cdot \frac{1}{\text{GAW}}$$

$$N_{\text{O}} = 1.499 \times 10^{21} \text{ cm}^{-3}$$

Lead has three naturally occurring isotopes which have different cross section data, so it is necessary to determine the density for each isotope. Pb206 and Pb207 each make up about 25% of naturally occurring isotopes while Pb208 accounts for the other 50%. Because the macroscopic cross section is proportional to the element density, the isotope densities are proportional to their naturally occurring abundance.

$$N_{\text{Pb206}} := N_{\text{Pb}} \cdot .25$$

$$N_{\text{Pb206}} = 8.08 \times 10^{20} \text{ cm}^{-3}$$

$$N_{\text{Pb207}} := N_{\text{Pb}} \cdot .25$$

$$N_{\text{Pb207}} = 8.08 \times 10^{20} \text{ cm}^{-3}$$

$$N_{\text{Pb208}} := N_{\text{Pb}} \cdot .5$$

$$N_{\text{Pb208}} = 1.616 \times 10^{21} \text{ cm}^{-3}$$

Appendix D: Total Dose Calculation

An example of the dose calculation is done for the isotope Pb-206. Calculations were performed as described in equation 8.

A differential flux distribution was obtained from OSU for their research reactor running at 300 kW and converted to a group flux distribution as shown in columns 1 and 2 of figure 71.

OSU Energy Group (eV)	Neutron Energy Group Flux (300 kW)	Group Energy Flux (J*cm ⁻² *s ⁻¹)	Parsed Pb206 Energy Group (eV)	Pb206 Cross Section (cm ²)	Multiply by atom density to get Pb206 Macro Cross Section (cm ⁻¹)	Pb206 MAC (cm ² /g) (macro cross sec / Pb density)	Average energy loss from neutron scatter (Qmax/2)(Turner p.218)	Dose Rate at 300 kW (J*g ⁻¹ *s ⁻¹)	Dose Rate (Mrad / s)	Total Dose Rate at 300 kW (Mrad / s)
1.00E-04	0.00E+00	0.00E+00	2.53E-02	2.39E-26	1.93E-05	2.94E-05	0.00961516	0.00E+00	0.00E+00	5.32E-07
1.05E-04	8.52E+05	1.43E-17	2.53E-02	2.39E-26	1.93E-05	2.94E-05	0.00961516	4.05E-24	4.05E-25	
1.10E-04	8.93E+05	1.57E-17	2.53E-02	2.39E-26	1.93E-05	2.94E-05	0.00961516	4.45E-24	4.45E-25	
1.15E-04	9.34E+05	1.72E-17	2.53E-02	2.39E-26	1.93E-05	2.94E-05	0.00961516	4.86E-24	4.86E-25	
1.20E-04	9.76E+05	1.87E-17	2.53E-02	2.39E-26	1.93E-05	2.94E-05	0.00961516	5.30E-24	5.30E-25	
1.27E-04	1.44E+06	2.92E-17	2.53E-02	2.39E-26	1.93E-05	2.94E-05	0.00961516	8.26E-24	8.26E-25	
1.35E-04	1.74E+06	3.76E-17	2.53E-02	2.39E-26	1.93E-05	2.94E-05	0.00961516	1.06E-23	1.06E-24	
1.42E-04	1.61E+06	3.66E-17	2.53E-02	2.39E-26	1.93E-05	2.94E-05	0.00961516	1.04E-23	1.04E-24	
1.50E-04	1.94E+06	4.66E-17	2.53E-02	2.39E-26	1.93E-05	2.94E-05	0.00961516	1.32E-23	1.32E-24	
2.55E-02	2.31E+10	9.41E-11	1.00E+00	3.80E-27	3.07E-06	4.68E-06	0.00961516	4.23E-18	4.23E-19	
2.76E-02	2.31E+10	9.96E-11	1.00E+00	3.80E-27	3.07E-06	4.68E-06	0.00961516	4.48E-18	4.48E-19	
2.80E-02	1.53E+10	6.86E-11	1.00E+00	3.80E-27	3.07E-06	4.68E-06	0.00961516	3.09E-18	3.09E-19	

Figure 71. Pb206 dose rate calculation at 300 kW.

In column 3 the group energy is multiplied by the group flux to create a group energy flux (eV/cm²-s) and then converted from electron volts to joules. The ENDF file for Pb-206 has been organized to match the mesh of the OSU energy flux distribution. Neutron group energies less than or equal to the Pb-206 group energy are aligned to correspond with the appropriate cross section. On row 10 the neutron group energy exceeds the lead group energy so the next higher energy group of the Pb-206 ENDF mesh is used. In column 6, the atom density calculated in Appendix C is used to convert the microscopic cross section to the macroscopic cross section. Column 7 shows the average

fraction of energy that can be transferred to the nucleus by a neutron as described by equation 11 (Turner, 1995, 218):

$$Q_{ave} = \frac{2mME_n}{(M + m)^2} \quad (11)$$

The dose rate is then determined as the product of the group energy flux, the macroscopic cross section divided by density, and the average energy fraction as described with equation 8. The last column is the sum of all dose rates at each energy group.

Flux is proportional to the power of the reactor; therefore the dose rate at any power is also proportional. The dose rate at 300 kW was calculated in the figure 71, so the dose rate for all other power settings used during the experiment is shown in figure 72. The total time of transducer exposure at each dose rate is used to calculate the total dose for Pb-206.

Power	Dose rate (Mrad/s)	Total time at dose rate (sec)	Dose (Mrad)	1 Mrad=1E5 Gy 1 Gy=1 J/Kg
300 kW	5.32E-07	3600	0.001916	
50 kW	8.87E-08	11220	0.000995	
100 kW	1.77E-07	8400	0.00149	
200 kW	3.55E-07	4800	0.001703	
450 kW	7.98E-07	53400	0.042631	
		Total:	0.048735	

Figure 72. Pb206 dose calculation at all powers used in reactor.

Finally, the total dose is determined by adding the individual dose for each atom and isotope in a lead Metaniobate crystal cell. Figure 73 shows the total dose calculation.

	Mrad	Gy (J/Kg)
Nb	0.074509	7.45092E+03
O	0.173118	1.73118E+04
Pb206	0.048735	4.87353E+03
Pb207	0.048902	4.89019E+03
Pb208	0.047162	4.71622E+03
Total:	0.392427	3.92427E+04
	392 krad	39.2 kGy

Figure 73. Total dose to lead metaniobate.

Appendix E: Rate of Heating for Lead Metaniobate

To determine heating rate in the lead metaniobate due to radiation interaction, I use dose rate at 300 kW and specific heat.

$$C_v := 0.31 \cdot \frac{\text{J}}{\text{gm} \cdot \text{K}}$$

specific heat for lead metaniobate
(Admiralty Materials Laboratory
publication, fig. 16)

$$\text{Doserate} := 4.29 \cdot 10^{-1} \cdot \frac{\text{Gy}}{\text{s}}$$

dose rate using **total cross sections**.

$$\frac{\text{Doserate}}{C_v} = 1.384 \times 10^{-3} \frac{\text{K}}{\text{s}}$$

1 degree every 723 seconds.

At max reactor power (450 kW), the dose rate would be:

$$\frac{450}{300} \cdot \text{Doserate} = 0.644 \frac{\text{J}}{\text{kg} \cdot \text{s}}$$

And heating would be:

$$\frac{\frac{450}{300} \cdot \text{Doserate}}{C_v} = 2.076 \times 10^{-3} \frac{\text{K}}{\text{s}}$$

1 degree every 482 seconds.

a back of the envelope calculation for the heating effects on stainless steel using only the thermal spectrum (0.4 eV, Turner p. 222) and the thermal cross section for steel of 3 barns (Handbook of Applied Eng. Science, p. 432).

$$\text{Doserate} := 3.1 \cdot 10^{-6} \cdot \frac{\text{Gy}}{\text{s}}$$

$$C_v := 0.502 \cdot \frac{\text{J}}{\text{gm} \cdot \text{K}}$$

(Handbook of Applied Eng.
Science, p. 432).

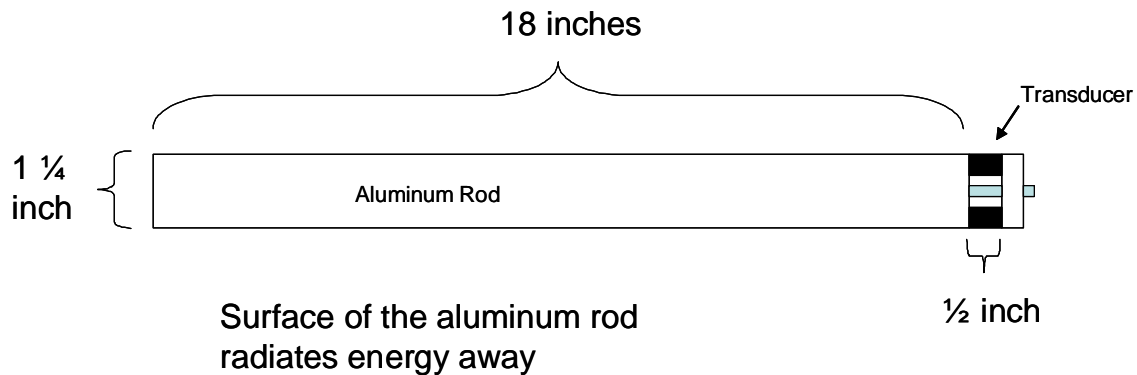
$$\frac{\text{Doserate}}{C_v} = 6.175 \times 10^{-9} \frac{\text{K}}{\text{s}}$$

again, **negligible heating of the steel case** due to thermal neutrons.

Appendix F: Heat Transfer Calculations

To approximate the temperature increase inside the transducers during irradiation, the dose rate (J/kg-s) is used to determine the rate at which energy is being deposited into the transducer. The energy manifests itself as heat and conductively flows into the aluminum rod. Equation 10 is then used to graph the rate at which heat is radiated away from the aluminum rod as a function of the surface temperature of the rod. An assumption made in this model is that the rate of conductive heat transfer from the transducer to the aluminum rod is negligible in comparison to the radiative heat transfer rate to the surrounding air.

Heat source inside each $\frac{1}{2}$ inch transducer is a 85 mm^3 lead metaniobate crystal



$$\text{Doserate} := 0.644 \cdot \frac{\text{J}}{\text{kg} \cdot \text{s}}$$

Dose rate at 450kW.

See Appendix D

$$\rho := 6.2 \cdot \frac{\text{gm}}{\text{cm}^3}$$

Density of lead metaniobate.

Quantity of energy input to system by 3 lead metaniobate transducer elements:

$$h := .3 \cdot \text{cm}$$

$$r := .3 \cdot \text{cm}$$

$$\text{vol} := h \cdot \pi r^2$$

$$\text{Vol}_{\text{total}} := 3 \cdot \text{vol}$$

$$\text{LMN}_{\text{mass}} := \rho \cdot \text{Vol}_{\text{total}}$$

$$\text{LMN}_{\text{mass}} = 1.578 \times 10^3 \text{ mg}$$

$$\text{Energy}_{\text{in}} := \text{Doserate} \cdot \text{LMN}_{\text{mass}}$$

$$\text{Energy}_{\text{in}} = 1.016 \times 10^{-3} \frac{\text{J}}{\text{s}}$$

Now determine temperature at which radiative cooling is the same as Energy flowing into the system.

$$\sigma := 9.733 \times 10^{-9} \cdot \frac{\text{J}}{\text{s} \cdot \text{m}^2 \cdot \text{K}}$$

Stefan-Boltzmann Constant

$$\varepsilon := 0.1$$

Emissivity (dimensionless....reference internet....ranged from 0.1-0.3 for Aluminum)

$$T_{\text{infinity}} := 303 \cdot \text{K}$$

Temperature of heat sink (reactor pool) was approx. 30 deg. C.

$$\text{length} := 18 \cdot \text{in}$$

$$\text{diameter} := \frac{5}{4} \cdot \text{in}$$

Dimensions of radiative cooling portion of waveguide.

$$\text{perimeter} := \pi \cdot \text{diameter}$$

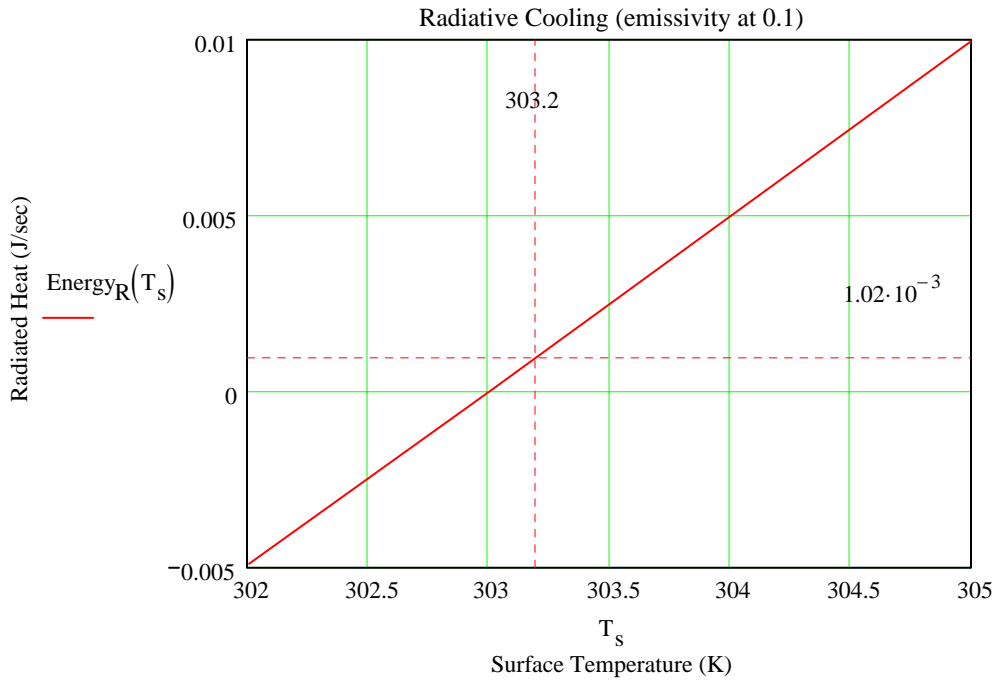
$A := \text{length} \cdot \text{perimeter}$

$$A = 0.046\text{m}^2$$

Surface area of cooling portion of waveguide.

Radiative Cooling: $\text{Energy}_R(T_s) := \sigma \cdot \epsilon \cdot A \cdot (T_s^4 - T_{\text{infinity}}^4)$

Plotting the radiative energy transfer rate as a function of surface temperature, the temperature that radiates energy at the same rate as it is being internally generated by the dose to the lead metaniobate can be found.



Bibliography

- “Acoustic Emission,” Tutorial on technology, n. pag., 23 Jan 2004
http://www.twi.co.uk/j32k/protected/band_3/ksndt005.html.
- “Force Sensors,” Tutorial on sensors. n. pag., 4 Nov 2003
<http://www.omega.com/literature/transactions/volume3/force.html>.
- “Infrared Measurement,” Tutorial on blackbody radiation. n. pag., 15 Feb 2004
<http://www.electro-optical.com>
- “Lead Metaniobate,” Retailer product description. n. pag., 6 Nov 2003
<http://www.piezo-kinetics.com/pn.htm>.
- “Piezoelectric Ceramic,” Retailer product description. n. pag., 4 Nov 2003
<http://www.piezotechnologies.com/k81.htm>.
- “Piezoelectric Transducers,” Tutorial on transducers. n. pag., 5 Nov 2003
<http://www.ndt-ed.org/EducationResources/CommunityCollege/Ultrasonics/equipmentTrans/piezotransducers.htm>.
- “Piezoelectricity,” Retailer product description and theory. n. pag., 22 Jan 2004
http://www.americanpiezo.com/piezo_theory/Index.htm.
- Broomfield, G. H. *The Effects of Temperature and Irradiation on Piezoelectric Acoustic Transducers and Materials*. Harwell Laboratory, December 1985.
- Etherington, Harold. *Nuclear Engineering Handbook*. New York: McGraw-Hill Book Company, 1958.
- Gover J. E., and Srour J. R. “Basic Radiation Effects in Nuclear Power Electronics Technology.” Sandia National Laboratories, April 1986.
- Halverson, S. L., T. T. Anderson, A. P. Gavin, and T. Grate. “Radiation Exposure of a Lithium Niobate Crystal at High Temperatures,” *IEEE Transactions on Nuclear Science*, vol. NS-17, Dec. 1970.
- Holbert, K. E., S. Sankaranarayanan, S. S. McCready, D. R. Spearing, A. S. Heger. *Response of Piezoelectric Acoustic Emission Sensors to Gamma Radiation*, Conference RADECS 2003.
- Holbert, Keith. E., Short course handout, “Radiation Effects on Piezoresistive and Piezoelectric Sensors.” Los Alamos National Lab, Los Alamos, New Mexico, January 2004.

- Holmes-Siedle, A., Adams, L. *Handbook of Radiation Effects*. Great Britain: Oxford University Press, 2002.
- Huth, Gerald C., "Conductivity Induced in Insulating Materials During Gamma Irradiation." Unknown publisher, Unknown date.
- Kerris, K. G. "Practical Dosimetry for Radiation Hardness Testing," *IEEE Nuclear and Space Radiation Effects Conference*. Louisiana: New Orleans, July 1992.
- Khazan, A. D. "Piezoelectric Force Transducer", *Transducers and Their Elements*. n. pag., Prentice Hall PTR. 5 Nov 2003
<http://zone.ni.com/devzone/conceptd.nsf/webmain/>.
- Kinsler, L. E., Frey, A. R. *Fundamentals of Acoustics 2nd Edition*. New York: John Wiley & Sons, Inc., 1962.
- Knoll, G. F., *Radiation Detection and Measurement 3rd Edition*. New York: John Wiley & Sons, Inc., 2000.
- Lane, R., Mack, D., Brown, K. R. *Dielectric, Piezoelectric and Pyroelectric Properties of the Lead Metaniobate-Barium Niobate System*. Admiralty Materials Laboratory, 1971.
- Ma, T. P., Dressendorfer, P. V., *Ionizing Radiation Effects in MOS Devices & Circuits*. New York: D. Van Nostrand Company Inc., 1950.
- Mason, W. P. *Piezoelectric Crystals and Their Application to Ultrasonics*. New York: D. Van Nostrand Company Inc., 1950.
- McCready, S., Harlow T., Heger A., and Holbert K. "Piezoresistive Micromechanical Transducer Operation in a Pulsed Neutron and Gamma Ray Environment." unpublished paper submitted to the IEEE Nuclear and Space Radiation Effects Conference, July 2002.
- Myers, G. E. *Analytical Methods in Conduction Heat Transfer*. New York: Genium Publishing Corporation, 1987.
- Parker, S. P. *McGraw-Hill Encyclopedia of Physics*. New York: McGraw-Hill Book Company, 1983.
- Parker, S. P. *Acoustics Source Book*. New York: McGraw-Hill Book Company, 1987.
- Smith, R. W. "Gamma Radiation Effects in Lithium Niobate," *Proceedings of the IEEE*, vol. 59, April 1971.

Srour, J. R., "Displacement Damage Effects in Electronic Materials, Devices, and Intergrated Circuits", *IEEE Nuclear and Space Radiation Effects Conference*, 11 July 1988.

Turner, J. E. *Atoms, Radiation, and Radiation Protection*. New York: John Wiley & Sons Inc., 1995.

Willmon, S. J. *Total Dose Effects of Ionizing and Non-Ionizing Radiation on Piezoresistive Pressure Transducer Chips*. MS Thesis, AFIT/GNE/ENP/03-11. Air Force Institute of Technology, Wright-Patterson AFB, OH, March 2003.

Vita

Major Michael R. Severson graduated from Northwest Nazarene University at Nampa, Idaho with a Bachelor of Science degree in Chemistry. Following his commissioning as a second lieutenant of Aviation, he was assigned to 2nd Battalion, 229th Attack Helicopter Regiment in Fort Rucker, Alabama. While in Alabama, he served as an aeroscout platoon leader, maintenance company executive officer, and headquarters staff officer.

Following completion of the Aviation Officer Advanced Course at Fort Rucker, Alabama, Major Severson was assigned as the aircraft maintenance production control officer, aircraft subsystems platoon leader, and aircraft maintenance platoon leader for the 4st Battalion, 123rd Aviation Regiment at Fort Wainwright, Alaska.

On his next assignment, Major Severson assumed command of Headquarters Company, 78th Aviation Battalion in Camp Zama, Japan. Sixteen months later he assumed command of D Company, 78th Aviation Battalion, where he was responsible for the battalion aircraft maintenance program.

After completing his command tour, Major Severson entered the Graduate School of Engineering at the Air Force Institute of Technology at Wright-Patterson Air Force Base, Ohio. Upon graduation, he will be assigned to the Defense Threat Reduction Agency.

REPORT DOCUMENTATION PAGE				Form Approved OMB No. 074-0188	
<p>The public reporting burden for this collection of information is estimated to average 1 hour per response, including the time for reviewing instructions, searching existing data sources, gathering and maintaining the data needed, and completing and reviewing the collection of information. Send comments regarding this burden estimate or any other aspect of the collection of information, including suggestions for reducing this burden to Department of Defense, Washington Headquarters Services, Directorate for Information Operations and Reports (0704-0188), 1215 Jefferson Davis Highway, Suite 1204, Arlington, VA 22202-4302. Respondents should be aware that notwithstanding any other provision of law, no person shall be subject to a penalty for failing to comply with a collection of information if it does not display a currently valid OMB control number.</p> <p>PLEASE DO NOT RETURN YOUR FORM TO THE ABOVE ADDRESS.</p>					
1. REPORT DATE (mm-yyyy) March 2004		2. REPORT TYPE Master's Thesis		3. DATES COVERED (From – To) June 2003 – March 2004	
4. TITLE AND SUBTITLE AN EXPERIMENTAL DESIGN FOR MEASURING IN SITU RADIATION DAMAGE TO A PIEZOELECTRIC TRANSDUCER				5a. CONTRACT NUMBER	
				5b. GRANT NUMBER	
				5c. PROGRAM ELEMENT NUMBER	
6. AUTHOR(S) Severson, Michael R., Major, USA				5d. PROJECT NUMBER	
				5e. TASK NUMBER	
				5f. WORK UNIT NUMBER	
7. PERFORMING ORGANIZATION NAMES(S) AND ADDRESS(S) Air Force Institute of Technology Graduate School of Engineering and Management 2950 Hobson Way, Building 640 WPAFB OH 45433-7765				8. PERFORMING ORGANIZATION REPORT NUMBER AFIT/GNE/ENP/04-06	
9. SPONSORING/MONITORING AGENCY NAME(S) AND ADDRESS(ES) DTRA HEADQUARTERS ATTN: Mr. Gerry Baird DTRA/CSNP 8725 John J. Kingman Road Ft. Belvoir, VA 22060-6201				10. SPONSOR/MONITOR'S ACRONYM(S)	
				11. SPONSOR/MONITOR'S REPORT NUMBER(S)	
12. DISTRIBUTION/AVAILABILITY STATEMENT APPROVED FOR PUBLIC RELEASE; DISTRIBUTION UNLIMITED.					
13. SUPPLEMENTARY NOTES					
14. ABSTRACT <p>An experiment was conducted investigating the use of an acoustic pulse waveguide to collect response measurements from three piezoelectric acoustic emission (AE) transducers while the transducers were exposed to an active nuclear reactor neutron flux ranging from 1×10^{11} to 2.4×10^{12} neutrons per $\text{cm}^2 \text{ s}$. Discrete frequency pulses generated by an Arbitrary Waveform Generator were transmitted by an aluminum waveguide to the core of the Ohio State University Research Reactor (OSURR). Three AE transducers coupled to the waveguide were exposed to the reactor neutron fluence and their response to each frequency pulse was measured over time. The recorded data was used to study the correlation between the neutron dose and resulting device damage</p> <p>Data sampling of transducer response was reproducible with a standard deviation that ranged between 3% and 8% of the mean value for all frequencies. Final transducer response levels varied between devices and frequencies, but were consistently degraded. Decreases in response between transducers ranged from 36% to 78% using the average percent decrease over ten test frequencies.</p>					
15. SUBJECT TERMS Lead Metaniobate, Piezoelectric Materials, Piezoelectric Transducers, Neutron Irradiation, Radiation Damage					
16. SECURITY CLASSIFICATION OF:			17. LIMITATION OF ABSTRACT	18. NUMBER OF PAGES	19a. NAME OF RESPONSIBLE PERSON
a. REPORT	b. ABSTRACT	c. THIS PAGE			James C. Petrosky, LTC, USA
U	U	U	UU	114	19b. TELEPHONE NUMBER (Include area code) (937) 255-3636, ext 4562 (james.petrosky@afit.edu)